Research Article

Afzaal Mubashir Hayat, Muhammad Abbas, Farah Aini Abdullah, Tahir Nazir, Hamed Ould Sidi, Homan Emadifar, and Amani Alruwaili*

Numerical solutions of generalized Atangana–Baleanu time-fractional FitzHugh–Nagumo equation using cubic B-spline functions

https://doi.org/10.1515/phys-2023-0120
received July 31, 2023; accepted January 10, 2024

Abstract: The generalization of the classical FitzHugh–Nagumo model provides a more accurate description of the physical phenomena of neurons by incorporating both nonlinearity and fractional derivatives. In this article, we present a numerical method for solving the time-fractional FitzHugh–Nagumo equation (TFFNE) in the sense of the Atangana–Baleanu fractional derivative using B-spline functions. The proposed method employs a finite difference scheme to discretize the fractional derivative in time, while θ-weighted scheme is used to discretize the space directions. The efficiency of the scheme is demonstrated through numerical results and rate of convergence. The convergence order and error norms are studied at different values of the noninteger parameter, temporal directions, and spatial directions. Finally, the effectiveness of the proposed methodology is examined through the analysis of three applications.

Keywords: computational physics, nonlinear time-fractional FitzHugh–Nagumo equation, Atangana–Baleanu fractional derivative, cubic B-spline functions, finite difference formulation, convergence and stability

*** Corresponding author: Amani Alruwaili,** Department of Physics, College of Science, Northern Border University, Arar, Saudi Arabia, e-mail: amani.sayer@nbu.edu.sa
Afzaal Mubashir Hayat, Tahir Nazir: Department of Mathematics, University of Sargodha, 40100 Sargodha, Pakistan
Muhammad Abbas: Department of Mathematics, University of Sargodha, 40100 Sargodha, Pakistan, e-mail: muhammad.abbas@uos.edu.pk
Farah Aini Abdullah: School of Mathematical Sciences, Universiti Sains Malaysia, 11800 Penang, Malaysia
Hamed Ould Sidi: Department of Mathematics, Faculty of Sciences, University of Nouakchott Al Aasriya, Nouakchott Bp 6093, Mauritania
Homan Emadifar: Department of Mathematics, Saveetha School of Engineering, Saveetha Institute of Medical and Technical Sciences, Saveetha University, Chennai-602 105, Tamil Nadu, India; MEU Research Unit, Middle East University, Amman, Jordan

1 Introduction

Splines hold a prominent position among mathematical functions frequently employed for estimation purposes. A spline is characterized as a piecewise polynomial function. In the realm of numerically interpreting ordinary differential equations, partial differential equations (PDEs), and fractional PDEs, the approach of utilizing spline functions for approximation has gained substantial popularity [1]. Fractional calculus has become a popular tool in many fields of research due to its ability to describe systems with memory, long-range dependence, and nonlocality. Traditional operators in fractional calculus have limitations. To address these issues, several researchers have proposed new operators or modifications to existing operators. The new operator developed by Caputo and Fabrizio [2] is nonsingular, which helps to alleviate this issue. However, this operator has a problem of nonlocality. The new operator developed by Atangana and Baleanu [3] helps to address both the nonlocality and the singularity issues associated with traditional operators, which makes it a valuable tool for researchers working with fractional calculus.

There are several implications for fractional derivatives in the areas of physics, mechanics, engineering, and biology [4]. In recent developments, with the use of fractional derivatives, the financial [5] and economic processes [6] have been described. Many interpretations of fractional derivatives exist, such as the geometric approach [7], informatic interpretation [8], and the economic approach [9]. Applications of fractional calculus include non-Newtonian fluid dynamics [10], rheology [11], hysteretic phenomena [12], and abnormal diffusion [13]. Studying the analytical or numerical approaches to fractional differential equations (FDEs) is extremely important since the majority of these issues may be stated as FDEs.

The FitzHugh–Nagumo equation (FNE) system has been derived by both FitzHugh [14] and Nagumo *et al.* [15]. Its simplicity and ability to capture key dynamics make it a

valuable tool in the study of nonlinear dynamical systems and the analysis of biological phenomena related to excitation and signal propagation. The time-fractional FNE that combines diffusion and nonlinearity has attracted the interest of many scientists in the fields of neurophysiology, logistical population increase, flame spread, catalytic chemical reaction, and nuclear reactor theory, as presented in the study by Injrou *et al.* [16].

Nonlinear inhomogeneous time-fractional FitzHugh–Nagumo PDE is considered as in [17],

$$\frac{\partial^{\gamma} p(z,t)}{\partial t^{\gamma}} = \nu \frac{\partial^2 p(z,t)}{\partial z^2} + \beta p(z,t)(1 - p^q(z,t))(p^q(z,t) - \eta) + U(z,t), a \le z \le b, \ t \in [t_0, T], \tag{1.1}$$

with initial condition (IC)

$$p(z, t_0) = \varepsilon(z) \tag{1.2}$$

and boundary conditions (BCs)

$$p(a,t) = \zeta_1(t), \quad p(b,t) = \zeta_2(t), \tag{1.3}$$

where $0 < \gamma < 1$, $U(z,t)$ is source function, $\nu > 0$ is kinematic viscosity, and β, η, q are parameters that $\beta \ge 0$, $\eta \in (0,1)$, and $q > 0$. The $\frac{\partial^{\gamma}}{\partial t^{\gamma}} p(z,t)$ is taking in the sense of Atangana–Baleanu time-fractional derivative (ABTFD).

Gordon [18] used a collocation and Hopscotch finite difference scheme to approximate FNE. Dehghan *et al.* [19] have approximated FNE using a semi-analytic method. Keskin and Oturan [20] used reduced differential transform method to approximate PDEs. By using Adomian Decomposition Method, the exact solution has been founded by Momani and Odibat [21] of time-fractional Navier–Stokes equation. Ragab *et al.* [22] used homotopy analysis method to approximate time-fractional Navier–Stokes equation. A biological behavior of three-species predator–prey model involving Atangana–Baleanu fractional derivative was studied by Ghanbari *et al.* [23]. Approximate solution using redefined extended cubic B-spline of time-fractional telegraph equation is proposed by Amin *et al.* [24]. Liu *et al.* [25] constructed a shifted Grünwald–Letnikov scheme to discretize the Riesz derivative of the fractional FitzHugh–Nagumo model. Shih *et al.* [26] examined FNE with applications. Abbasbandy [27] founded the soliton solutions of FNE using the homotopy analysis scheme. The explicit solution of FNE was founded by Kakiuchi and Tchizawa [28]. Schonbek [29] examined the FNE with boundary problems. Yanagida [30] discussed the stability of traveling front solutions of FNE. A nonstandard difference method was proposed by Namjoo *et al.* [31]. Angadi [32] solved FNE by wavelet-based lifting methods. Olmos and Shizgal [33] developed a pseudo-spectral method to examine the FNE. Abdulazeez and Modanli [34] found analytic solution of fractional order pseudo-hyperbolic telegraph equation using modified double Laplace transform method. The effect of fractal-fractional Caputo–Fabrizio derivative on the analysis of tumor growth model is studied by [35]. Baleanu *et al.* [36] studied stability and dynamical analysis of generalized fractional model with a real case study. Ali *et al.* [37] solved FNE using Galerkin finite element approach. A polynomial differential quadrature method is used by Jiwari *et al.* [38] for the numerical solutions of the generalized FitzHugh–Nagumo.

The article is structured as follows: the ABTFD, Parseval's identity (PI), and CBSFs are presented in Section 2; Section 3 shows the newly developed scheme; Sections 4 and 5 display stability and convergence of proposed approach, respectively; the effectiveness and validity of the suggested technique are examined in Section 6; and finally, Section 7 summarizes the conclusion.

2 Preliminaries

Definition 1. The ABTFD $\frac{\partial^{\gamma}}{\partial t^{\gamma}} p(z,t)$ of order $\gamma \in (0,1)$ is presented by Atangana and Baleanu [3] as follows:

$$\frac{\partial^{\gamma}}{\partial t^{\gamma}} p(z,t) = \frac{AB(\gamma)}{1-\gamma} \int_0^t \frac{\partial}{\partial v} p(z,v) E_{\gamma} \times \left[-\frac{\gamma}{1-\gamma} (t-v)^{\gamma} \right] \mathrm{d}v, \tag{2.1}$$

where $AB(\gamma)$ is a normalized form of function that has the property $AB(\gamma = 0) = AB(\gamma = 1) = 1$. $E_{\gamma,\sigma}(z)$ is the Mittag-Leffler function (MLF) of two parameters with $E_{\gamma,1}(z) = E_{\gamma}(z)$, which is defined by Mittag-Leffler [39] as follows:

$$E_{\gamma,\sigma}(z) = \sum_{y=0}^{\infty} \frac{z^y}{\Gamma(\gamma y + \sigma)}.$$

Some properties of MLF by fixing γ and σ are as follows:

- $E_{1,1}(z) = e^z$,
- $E_{1,2}(z) = \frac{e^z - 1}{z}$,
- $E_{2,1}(z^2) = \cosh(z)$,
- $E_{2,1}(-z^2) = \cos(z)$,
- $E_{2,2}(z^2) = \frac{\sinh(z)}{z}$.

Definition 2. If $\hat{\Omega} \in L^2[a,b]$, then PI is given as follows [40]:

$$\sum_{n=-\infty}^{\infty} |\hat{\Omega}(n)|^2 = \int_a^b |\tilde{\Omega}(z)|^2 \mathrm{d}z, \tag{2.2}$$

where $\hat{\Omega}(n) = \int_a^b \tilde{\Omega}(z) e^{2\pi i n z} \mathrm{d}z$ is Fourier transform for all integers n.

2.1 Cubic B-spline basis functions

The spatial domain $[a, b]$ be divided into equal length of N subintervals with $h = \frac{b-a}{N}$ such that $\{a = z_0, z_1, \cdots z_N = b\}$ with $z_r < z_{r+1}$, where $z_r = hk + z_0$ and $r = 0(1)N$.

Now, let $P(z, t)$ be the CBSFs approach for $p(z, t)$, i.e.,

$$P(z, t) = \sum_{r=-1}^{N+1} \Psi_r^m(t)\hat{B}_r(z), \tag{2.3}$$

where control points $\Psi_r^m(t)$ to be calculated at every temporal stage and CBSFs are defined as follows:

$$\hat{B}_r(z) = \frac{1}{6h^3}\begin{cases} (z - z_{r-2})^3, & \text{if } z \in [z_{r-2}, z_{r-1}), \\ 3(z - z_{r-1})h^2 & \text{if } z \in [z_{r-1}, z_r), \\ \quad + 3(z - z_{r-1})^2 h & \\ \quad - 3(z - z_{r-1})^3 & \\ \quad + h^3, & \\ h^3 + 3h^2(z_{r+1} - z) & \text{if } z \in [z_r, z_{r+1}), \\ \quad + 3h(z_{r+1} - z)^2 & \\ \quad - 3(z_{r+1} - z)^3, & \\ (z_{r+2} - z)^3, & \text{if } z \in [z_{r+1}, z_{r+2}), \\ 0, & \text{otherwise}. \end{cases} \tag{2.4}$$

Numerous geometrical features, including the geometric invariability, symmetry, the convex hull characteristic, local support, nonnegativity, and the partition of unity, are preserved in the CBSFs [41,42]. In addition, $\hat{B}_{-1}, \hat{B}_0, \cdots, \hat{B}_{N+1}$ have been constructed. Equations (2.3) and (2.4) provide the following approximations:

$$\begin{cases} (P)_r^m = \left(\frac{1}{6}\right)\Psi_{r-1}^m + \left(\frac{4}{6}\right)\Psi_r^m + \left(\frac{1}{6}\right)\Psi_{r+1}^m, \\ (P_z)_r^m = \left(\frac{1}{2h}\right)\Psi_{r+1}^m + \left(-\frac{1}{2h}\right)\Psi_{r-1}^m, \\ (P_{zz})_r^m = \left(\frac{1}{h^2}\right)\Psi_{r-1}^m + \left(-\frac{2}{h^2}\right)\Psi_r^m + \left(\frac{1}{h^2}\right)\Psi_{r+1}^m. \end{cases} \tag{2.5}$$

3 Illustration of the scheme

Suppose $[0, T]$ the time domain be divided into M subintervals of equal length with $\Delta t = \frac{T}{M}$ using $\{0 = t_0, t_1, \cdots t_M = T\}$ with $t_m < t_{m+1}$, where $t_m = m\Delta t$ and $m = 0 : 1 : M$. The ABTFD in Eq. (1.1) is discretized at $t = t_{m+1}$ as in [42]:

$$\begin{aligned} &\frac{\partial^\gamma}{\partial t^\gamma} p(z, t_{m+1}) \\ &= \frac{AB(\gamma)}{1-\gamma} \int_0^{t_{m+1}} \frac{\partial}{\partial \upsilon} p(z, \upsilon) E_\gamma\left[-\frac{\gamma}{1-\gamma}(t_{m+1} - \upsilon)^\gamma\right] d\upsilon, \\ &0 < \gamma < 1, \\ &= \frac{AB(\gamma)}{1-\gamma} \sum_{v=0}^{m} \int_{t_v}^{t_{v+1}} \frac{\partial}{\partial \upsilon} p(z, \upsilon) E_\gamma\left[-\frac{\gamma}{1-\gamma}(t_{m+1} - \upsilon)^\gamma\right] d\upsilon. \end{aligned} \tag{3.1}$$

Utilizing forward difference formulation, Eq. (3.1) becomes

$$\begin{aligned} \frac{\partial^\gamma}{\partial t^\gamma} p(z, t_{m+1}) &= \frac{AB(\gamma)}{1-\gamma} \sum_{v=0}^{m} \frac{p(z, t_{v+1}) - p(z, t_v)}{\Delta t} \\ &\quad \times \int_{t_v}^{t_{v+1}} E_\gamma\left[-\frac{\gamma}{1-\gamma}(t_{m+1} - \upsilon)^\gamma\right] d\upsilon + \lambda_{\Delta t}^{m+1} \\ &= \frac{AB(\gamma)}{1-\gamma} \sum_{v=0}^{m} [p(z, t_{m-v+1}) - p(z, t_{m-v})] \\ &\quad \times \left\{(v+1)E_{\gamma,2}\left[-\frac{\gamma}{1-\gamma}((v+1)\Delta t)^\gamma\right]\right. \\ &\quad \left. - vE_{\gamma,2}\left[-\frac{\gamma}{1-\gamma}(v\Delta t)^\gamma\right]\right\} + \lambda_{\Delta t}^{m+1} \\ &= \frac{AB(\gamma)}{1-\gamma} \sum_{v=0}^{m} [p(z, t_{m-v+1}) - p(z, t_{m-v})]((v \\ &\quad + 1)E_{v+1} - vE_v) + \lambda_{\Delta t}^{m+1}. \end{aligned}$$

Hence,

$$\begin{aligned} \frac{\partial^\gamma}{\partial t^\gamma} p(z, t_{m+1}) = \frac{AB(\gamma)}{1-\gamma} &\sum_{v=0}^{m} w_v \\ &\times [p(z, t_{m-v+1}) - p(z, t_{m-v})] + \lambda_{\Delta t}^{m+1}, \end{aligned} \tag{3.2}$$

where $E_v = E_{\gamma,2}\left[-\frac{\gamma}{1-\gamma}(v\Delta t)^\gamma\right]$ and $w_v = (v+1)E_{v+1} - vE_v$. Simple observation reveals that

- $w_v > 0$ and $w_0 = E_1$, $v = 0 : 1 : m$,
- $w_0 > w_1 > w_2 > \cdots > w_v$, $w_v \to 0$ as $v \to \infty$,
- $\sum_{v=0}^{m}(w_v - w_{v+1}) + w_{m+1} = (E_1 - w_1) + \sum_{v=1}^{m-1}(w_v - w_{v+1}) + w_m = E_1$.

In addition, the truncation error $\lambda_{\Delta t}^{m+1}$ is shown in [43] as follows:

$$\begin{aligned}\lambda_{\Delta t}^{m+1} &= \frac{AB(\gamma)}{1-\gamma}\sum_{v=0}^{m}\int_{t_v}^{t_{v+1}}\frac{\Delta t}{2}\frac{\partial^2 p(z,t_v)}{\partial t^2}\\ &\quad\times E_\gamma\left[-\frac{\gamma}{1-\gamma}(t_{m+1}-\upsilon)^\gamma\right]\mathrm{d}\upsilon\\ &= \frac{AB(\gamma)}{1-\gamma}\frac{(\Delta t)^2}{2}\sum_{v=0}^{m}\frac{\partial^2 p(z,t_v)}{\partial t^2}\\ &\quad\times\left\{(m-v+1)E_{\gamma,2}\left[-\frac{\gamma}{1-\gamma}((m-v+1)\Delta t)^\gamma\right]\right.\\ &\quad\left.-(m-v)E_{\gamma,2}\left[-\frac{\gamma}{1-\gamma}((m-v)\Delta t)^\gamma\right]\right\}\\ &= \frac{AB(\gamma)}{1-\gamma}\frac{(\Delta t)^2}{2}\sum_{v=0}^{m}\frac{\partial^2 p(z,t_v)}{\partial t^2}\\ &\quad\times((m-v+1)E_{m-v+1}-(m-v)E_{m-v})\\ &\le \frac{AB(\gamma)}{1-\gamma}\frac{(\Delta t)^2}{2}\left[\max_{0\le t\le t_m}\frac{\partial^2 p(z,t)}{\partial t^2}\right]c_1,\end{aligned}$$

where c_1 is constant.

$$|\lambda_{\Delta t}^{m+1}| \le \vartheta(\Delta t)^2, \tag{3.3}$$

where Ψ is constant.

Now using θ-weighted scheme and Eq. (3.2), Eq. (1.1) becomes

$$\begin{aligned}&\frac{AB(\gamma)}{1-\gamma}\sum_{v=0}^{m}w_v[p(z,t_{m-v+1})-P(z,t_{m-v})]\\ &= \theta[\nu p_{zz}(z,t_{m+1})+\beta p(z,t_{m+1})(1\\ &\quad-p^q(z,t_{m+1}))(p^q(z,t_{m+1})-\eta)]\\ &\quad+(1-\theta)[\nu p_{zz}(z,t_m)\\ &\quad+\beta p(z,t_m)(1-p^q(z,t_m))(p^q(z,t_m)-\eta)]\\ &\quad+U(z,t_{m+1}).\end{aligned} \tag{3.4}$$

Discretizing Eq. (3.4) along spatial direction for $\theta = 1$ and using linearization formula as defined in [44], we obtain

$$(p^q)_r^{m+1} = q(p)_r^{m+1}(p^{q-1})_r^m - (q-1)(p^q)_r^m. \tag{3.5}$$

$$\begin{cases}(p^3)_r^{m+1} = 3(p)_r^{m+1}(p^2)_r^m - 2(p^3)_r^m,\\ (p^2)_r^{m+1} = 2(p)_r^{m+1}(p)_r^m - (p^2)_r^m.\end{cases} \tag{3.6}$$

Now using $q = 1$, we have

$$\begin{aligned}&[E_1-2\xi\beta(1+\eta)(p)_r^m+\xi\beta\eta+3\xi\beta(p^2)_r^m](p)_r^{m+1}\\ &\quad-\xi\nu(p_{zz})_r^{m+1}\\ &= E_1(p)_r^m-\xi\beta(1+\eta)(p^2)_r^m+2\xi\beta(p^3)_r^m\\ &\quad-\sum_{v=1}^{m}w_v((p)_r^{m-v+1}-(p)_r^{m-v})+\xi U_r^{m+1},\end{aligned} \tag{3.7}$$

where $\xi = \frac{1-\gamma}{AB(\gamma)}$, $p_k^m = p(z_r, t_m)$, and $U_r^{m+1} = U(z_r, t_{m+1})$.

Using Eq. (2.5) in Eq. (3.7), we obtain

$$\begin{aligned}&a_1\left[\frac{1}{6}\Psi_{r-1}^{m+1}+\frac{4}{6}\Psi_r^{m+1}+\frac{1}{6}\Psi_{r+1}^{m+1}\right]\\ &\quad-\varsigma\left[\frac{1}{h^2}\Psi_{r-1}^{m+1}-\frac{2}{h^2}\Psi_r^{m+1}+\frac{1}{h^2}\Psi_{r+1}^{m+1}\right]\\ &= \psi_1\left[\frac{1}{6}\Psi_{r-1}^{m}+\frac{4}{6}\Psi_r^{m}+\frac{1}{6}\Psi_{r+1}^{m}\right]\\ &\quad-\sum_{v=1}^{m}w_v\left[\frac{1}{6}(\Psi_{r-1}^{m-v+1}-\Psi_{r-1}^{m-v})\right.\\ &\quad\left.+\frac{4}{6}(\Psi_r^{m-v+1}-\Psi_r^{m-v})+\frac{1}{6}(\Psi_{r+1}^{m-v+1}-\Psi_{r+1}^{m-v})\right]\\ &\quad+\xi U_r^{m+1},\end{aligned} \tag{3.8}$$

$$\begin{aligned}&\left(\frac{1}{6}a_1-\frac{\varsigma}{h^2}\right)\Psi_{r-1}^{m+1}+\left(\frac{4}{6}a_1+\frac{2\varsigma}{h^2}\right)\Psi_r^{m+1}\\ &\quad+\left(\frac{1}{6}a_1-\frac{\varsigma}{h^2}\right)\Psi_{r+1}^{m+1}=Q_r^m\end{aligned} \tag{3.9}$$

$$f_r^m\Psi_{r-1}^{m+1}+g_r^m\Psi_r^{m+1}+H_r^m\Psi_{r+1}^{m+1}=Q_r^m, r=0:1:N, m=0:1:M, \tag{3.10}$$

where $a_1 = E_1 - 2\xi\beta(1+\eta)(p)_r^m + \xi\beta\eta + 3\xi\beta(p^2)_r^m$, $\varsigma = \xi\nu$, $f_r^m = \frac{1}{6}a_1 - \frac{\varsigma}{h^2}$, $g_r^m = \frac{4}{6}a_1 + \frac{2\varsigma}{h^2}$, $H_r^m = \frac{1}{6}a_1 - \frac{\varsigma}{h^2}$, $Q_r^m = \psi_1\left[\frac{1}{6}\Psi_{r-1}^m + \frac{4}{6}\Psi_r^m + \frac{1}{6}\Psi_{r+1}^m\right] - \sum_{v=1}^m w_v\left[\frac{1}{6}(\Psi_{r-1}^{m-v+1} - \Psi_{r-1}^{m-v}) + \frac{4}{6}(\Psi_r^{m-v+1} - \Psi_r^{m-v}) + \frac{1}{6}(\Psi_{r+1}^{m-v+1} - \Psi_{r+1}^{m-v})\right] + \xi U_r^{m+1}$, and $\psi_1 = E_1 - \xi\beta(1+\eta)(p)_r^m + 2\xi\beta(p^2)_r^m$. This system (Eq. (3.10)) has $N+1$ linear equations with $N+3$ unknowns. Two more equations can be found for unique solution from the given BCs (Eq. (1.3)).

$$\begin{cases}\frac{1}{6}\Psi_{-1}^{m+1}+\frac{4}{6}\Psi_0^{m+1}+\frac{1}{6}\Psi_1^{m+1}=\zeta_1^{m+1}\\ \frac{1}{6}\Psi_{N-1}^{m+1}+\frac{4}{6}\Psi_N^{m+1}+\frac{1}{6}\Psi_{N+1}^{m+1}=\zeta_2^{m+1}\end{cases} \tag{3.11}$$

Equations (3.10)–(3.11) equations have the following form of the matrix:

$$\begin{pmatrix} \frac{1}{6} & \frac{4}{6} & \frac{1}{6} & & & & & \\ f_0^m & g_0^m & H_0^m & & & & & \\ & f_1^m & g_1^m & H_1^m & & & & \\ & & \ddots & \ddots & \ddots & & & \\ & & & f_{N-1}^m & g_{N-1}^m & H_{N-1}^m & & \\ & & & & f_N^m & g_N^m & H_N^m & \\ & & & & \frac{1}{6} & \frac{4}{6} & \frac{1}{6} & \end{pmatrix} \begin{pmatrix} \Psi_{-1}^{m+1} \\ \Psi_0^{m+1} \\ \Psi_1^{m+1} \\ \vdots \\ \Psi_{N-1}^{m+1} \\ \Psi_N^{m+1} \\ \Psi_{N+1}^{m+1} \end{pmatrix} = \begin{pmatrix} \zeta_1^{m+1} \\ Q_0^{m+1} \\ Q_1^{m+1} \\ \vdots \\ Q_{N-1}^{m+1} \\ Q_N^{m+1} \\ \zeta_2^{m+1} \end{pmatrix}. \tag{3.12}$$

By using Eq. (1.2), the initial vector $\Psi^0 = [\Psi_{-1}^0, \Psi_0^0, \cdots, \Psi_{N+1}^0]^T$ is obtained as follows:

$$\begin{cases} (P_z)_r^0 = \varepsilon'(z_r), & r = 0, \\ (P)_r^0 = \varepsilon(z_r), & r = 0:1:N, \\ (P_z)_r^0 = \varepsilon'(z_r), & r = N. \end{cases} \tag{3.13}$$

The representation of the matrix form for the above system of equation is shown as

$$G\Psi^0 = R, \tag{3.14}$$

where

$$\begin{pmatrix} \frac{-1}{2h} & 0 & \frac{1}{2h} & & & & & \\ \frac{1}{6} & \frac{4}{6} & \frac{1}{6} & & & & & \\ & \frac{1}{6} & \frac{4}{6} & \frac{1}{6} & & & & \\ & & \ddots & \ddots & \ddots & & & \\ & & & \frac{1}{6} & \frac{4}{6} & \frac{1}{6} & & \\ & & & & \frac{1}{6} & \frac{4}{6} & \frac{1}{6} & \\ & & & & \frac{-1}{2h} & 0 & \frac{1}{2h} & \end{pmatrix} \begin{pmatrix} \Psi_{-1}^0 \\ \Psi_0^0 \\ \Psi_1^0 \\ \vdots \\ \Psi_{N-1}^0 \\ \Psi_N^0 \\ \Psi_{N+1}^0 \end{pmatrix} = \begin{pmatrix} \varepsilon'(z_0) \\ \varepsilon(z_0) \\ \varepsilon(z_1) \\ \vdots \\ \varepsilon(z_{N-1}) \\ \varepsilon(z_N) \\ \varepsilon'(z_N) \end{pmatrix}. \tag{3.15}$$

Any numerical algorithm can be used to solve Eq. (3.15). Mathematica 10 is used to conduct the numerical results.

4 The stability

The numerical technique is assumed to be stable when the error does not increase during the computing process [45]. Fourier method [46–48] is applied for the stability of proposed scheme. Now, let τ_r^m and $\tilde{\tau}_r^m$ represent the amplification component and its computation in Fourier transform, respectively κ_r^m is the error that can be addressed as follows:

$$\kappa_r^m = \tau_r^m - \tilde{\tau}_r^m, m = 1:1:M, r = 1:1:N-1.$$

Taking source function $U(z,t) = 0$ in Eq. (3.8), Eq. (3.8) becomes

$$\begin{aligned} f_r^m \Psi_{r-1}^{m+1} + g_r^m \Psi_r^{m+1} + H_r^m \Psi_{r+1}^{m+1} &= b_1 \Psi_{r-1}^m + b_2 \Psi_r^m + b_3 \Psi_{r+1}^m \\ &\quad - \sum_{v=1}^{m} w_v \Big[\frac{1}{6} (\Psi_{r-1}^{m-v+1} - \Psi_{r-1}^{m-v}) \\ &\quad + \frac{4}{6} (\Psi_r^{m-v+1} - \Psi_r^{m-v}) + \frac{1}{6} (\Psi_{r+1}^{m-v+1} - \Psi_{r+1}^{m-v}) \Big], \end{aligned} \tag{4.1}$$

where $b_1 = \frac{\psi_1}{6}$, $b_2 = \frac{4\psi_1}{6}$, and $b_3 = \frac{\psi_1}{6}$. From IC and BCs, we can write

$$\Psi_r^0 = \varepsilon(z_r), \quad r = 1:1:N \tag{4.2}$$

and

$$\Psi_0^m = \zeta_1(t_m), \quad \Psi_N^m = \zeta_2(t_m), \quad m = 0:1:M. \tag{4.3}$$

Define grid function as follows:

$$\Psi^m = \begin{cases} \Psi_r^m, z \in \left(z_r - \frac{h}{2}, z_r + \frac{h}{2} \right], & r = 1:1:N-1, \\ 0, z \in \left[a, a + \frac{h}{2} \right] \quad or \quad z \in \left[b - \frac{h}{2}, b \right]. \end{cases} \tag{4.4}$$

The function $\Psi^m(z)$ in the Fourier mode can be presented as follows:

$$\Psi^m(z) = \sum_{n=-\infty}^{\infty} \mathcal{F}^m(n) e^{\frac{2\pi t n z}{b-a}}, \tag{4.5}$$

where

$$\mathcal{F}^m(n) = \frac{1}{b-a} \int_a^b \Psi^m(z) e^{\frac{-2\pi t n z}{b-a}} dz, \quad m = 0(1)M \text{ and } \Psi^m = [\Psi_1^m, \Psi_2^m, \ldots, \Psi_{N-1}^m]^T. \tag{4.6}$$

Applying $\|.\|_2$ norm, we acquire

$$||\Psi^m||_2 = \sqrt{h\sum_{r=1}^{N-1}|\Psi_r^m|^2}$$
$$= \left(\int_a^{a+\frac{h}{2}}|\Psi^m|^2\mathrm{d}z + \sum_{k=1}^{N-1}\int_{z_k-\frac{h}{2}}^{z_r+\frac{h}{2}}|\Psi^m|^2\mathrm{d}z + \int_{b-\frac{h}{2}}^{b}|\Psi^m|^2\mathrm{d}z\right)^{\frac{1}{2}}$$
$$= \left(\int_a^b|\Psi^m|^2\mathrm{d}z\right)^{\frac{1}{2}}.$$

From Eq. (2.2), we have [40]

$$\int_a^b|\Psi^m|^2\mathrm{d}z = \sum_{n=-\infty}^{\infty}|\mathcal{F}^m(n)|^2.$$

Hence, we acquire

$$||\Psi^m||_2^2 = \sum_{n=-\infty}^{\infty}|\mathcal{F}^m(n)|^2. \tag{4.7}$$

Consider Eqs (4.1)–(4.3) present a solution in Fourier series as follows:

$$\Psi_r^m = \mathcal{F}^m e^{iarh}, \tag{4.8}$$

where $i = \sqrt{-1}$ and α is a real. Using Eq. (4.8) in Eq. (4.1), we obtained

$$\begin{aligned} f_r^m\mathcal{F}^{m+1}e^{-iah} + g_r^m\mathcal{F}^{m+1} + H_r^m\mathcal{F}^{m+1}e^{iah} &= b_1\mathcal{F}^m e^{-iah} + b_2\mathcal{F}^m + b_3\mathcal{F}^m e^{iah} \\ &\quad - \sum_{v=1}^{m} w_v\left[\frac{1}{6}(\mathcal{F}^{m-v+1}e^{-iah} - \mathcal{F}^{m-v}e^{-iah})\right. \\ &\quad + \frac{4}{6}(\mathcal{F}^{m-v+1} - \mathcal{F}^{m-v}) \\ &\quad \left. + \frac{1}{6}(\mathcal{F}^{m-v+1}e^{iah} - \mathcal{F}^{m-v}e^{iah})\right]. \end{aligned} \tag{4.9}$$

Utilizing the relation $e^{iah} + e^{-iah} = 2\cos(ah)$ and values of $b_1, b_2, b_3, f_r^m, g_r^m$, and H_r^m we obtain the following equality:

$$\mathcal{F}^{m+1} = \frac{\mathcal{F}^m\frac{\psi_1}{6}(2\cos(ah)+4)}{(2\cos(ah)+4)\frac{a_1}{6} + \frac{2\varsigma(1-\cos(ah))}{h^2}} - \frac{(2\cos(ah)+4)\sum_{v=1}^{m}\frac{w_v}{6}[\mathcal{F}^{m-v+1} - \mathcal{F}^{m-v}]}{(2\cos(ah)+4)\frac{a_1}{6} + \frac{2\varsigma(1-\cos(ah))}{h^2}} \tag{4.10}$$

$$\mathcal{F}^{m+1} = \frac{1}{\frac{a_1}{\psi_1} + \frac{24\varsigma\sin^2(\frac{rh}{2})}{\psi_1h^2(2\cos(rh)+4)}} \times \left[\mathcal{F}^m - \frac{\sum_{v=1}^{m}w_v[\mathcal{F}^{m-v+1} - \mathcal{F}^{m-v}]}{\psi_1}\right] \tag{4.11}$$

$$\mathcal{F}^{m+1} = \frac{\mathcal{F}^m}{\sigma_1} - \sum_{v=1}^{m}w_v\frac{\mathcal{F}^{m-v+1} - \mathcal{F}^{m-v}}{\psi_1\sigma_1}, \tag{4.12}$$

where $\sigma_1 = \frac{a_1}{\psi_1} + \frac{24\varsigma\sin^2\left(\frac{rh}{2}\right)}{\psi_1h^2(2\cos(rh)+4)}$ where $\psi_1 > 0$ and $a_1 > 0$. Obviously $\sigma_1 \geq 1$.

Lemma 4.1. *If $\mathcal{F}^m$ is the solution of Eq.* (4.12)*, then $|\mathcal{F}^m| \leq |\mathcal{F}^0|$, $m = 0(1)M$.*

Proof. To prove this lemma, we use mathematical induction. So, for $m = 0$, Eq. (4.12) reveals

$$|\mathcal{F}^1| = \frac{1}{\sigma_1}|\mathcal{F}^0| \leq |\mathcal{F}^0|, \quad \sigma_1 \geq 1.$$

Assume that $|\mathcal{F}^m| \leq |\mathcal{F}^0|$ for $m = 1, 2, \ldots, M-1$, then

$$\begin{aligned} |\mathcal{F}^{m+1}| &\leq \frac{1}{\sigma_1}|\mathcal{F}^m| - \frac{1}{\sigma_1\psi_1}\sum_{v=1}^{m}w_v(|\mathcal{F}^{m-v+1}| - |\mathcal{F}^{m-v}|) \\ &\leq \frac{1}{\sigma_1}|\mathcal{F}^0| - \frac{1}{\sigma_1\psi_1}\sum_{v=1}^{m}w_v(|\mathcal{F}^0| - |\mathcal{F}^0|) \\ &\leq |\mathcal{F}^0|. \end{aligned}$$

□

Theorem 1. *The proposed technique* (*Eq.* (3.10)) *is stable unconditionally.*

Proof. Using Lemma 4.1 and Eq. (4.7), we obtain

$$||\Psi^m||_2 \leq |\Psi^0|_2 \quad \forall m = 0, 1, \ldots, M.$$

This lemma shows that the developed approach is stable unconditionally. □

5 The convergence

The methodology as in [49] is used to analyze the convergence of the propagated approach. Initially, Theorem 2 is presented [50,51]:

Theorem 2. *Suppose U belongs to $C^2[a, b]$ and $P(z, t)$ belongs to $C^4[a, b]$, also partition of $[a, b]$ is $\mathfrak{O} = \{a = z_0, z_1, \cdots z_N = b\}$ with $z_r < z_{r+1}$ such that $z_r - a = hr$, where $k = 0 : 1 : N$. If solution curve is interpolated by unique spline $\tilde{P}(z, t)$ at $z_r \in \mathfrak{O}$, then for every $t \geq 0$, there is a constant ϖ_k independent of h, and for $r = 0, 1, 2$,* we have

$$||D^r(\tilde{P}(z, t) - p(z, t))||_\infty \leq \varpi_r h^{4-r}. \tag{5.1}$$

Lemma 5.1. *The CBSFs $\{\hat{B}_{-1}, \hat{B}_0, \ldots, \hat{B}_{N+1}\}$ in Eq.* (2.4) *fulfills the inequality as given in* [42]

$$\sum_{r=-1}^{N+1} |\hat{B}_r(z)| \le \frac{5}{3}, \quad 0 \le z \le 1. \tag{5.2}$$

Theorem 3. *The numerical approach $P(z,t)$ to the analytic solution $p(z,t)$ for the the time-fractional FitzHugh–Nagumo equation (TFFNE) (Eqs (1.1)–(1.3)) exists. In addition, if source function $U(z,t)$ belongs to $C^2[0,1]$ as in [42], then*

$$\|p(z,t) - P(z,t)\|_\infty \le \widetilde{\varpi} h^2, \quad \text{for all } t \ge 0, \tag{5.3}$$

for suitably small h, and $\widetilde{\varpi} > 0$ is independent of h.

Proof. Let $P(z,t) = \sum_{r=-1}^{N+1} V_r^m(t)\hat{B}_r(z)$ be the estimated spline for $p(z,t)$. Through the triangular inequality, we obtain

$$\|P(z,t) - p(z,t)\|_\infty \le \|\tilde{P}(z,t) - p(z,t)\|_\infty + \|\tilde{P}(z,t) - p(z,t)\|_\infty.$$

We have from the help of Theorem 2,

$$\|p(z,t) - P(z,t)\|_\infty \le \varpi_0 h^4 + \|\tilde{P}(z,t) - p(z,t)\|_\infty. \tag{5.4}$$

For the developed scheme, these $LP(z_r,t) = Lp(z_r,t) = U(z_r,t)$, where $r = 0,1,\dots,N$ are the conditions of collocation. Suppose that

$$L\tilde{P}(z,t) = \tilde{U}(z_r,t), r = 0(1)N.$$

Thus, $L(\tilde{p}(z_r,t) - p(z_r,t))$ can be indicated for any time level as

$$\begin{aligned}
&\left(\frac{a_1}{6} - \frac{\varsigma}{h^2}\right)\Phi_{r-1}^{m+1} + \left(\frac{4a_1}{6} + \frac{2\varsigma}{h^2}\right)\Phi_r^{m+1} + \left(\frac{a_1}{6} - \frac{\varsigma}{h^2}\right)\Phi_{r+1}^{m+1} \\
&= \frac{\psi_1}{6}\Phi_{r-1}^m + \frac{4\psi_1}{6}\Phi_r^m - \frac{\psi_1}{6}(\Phi_{r+1}^m) + \frac{\xi}{h^2}\rho_r^{m+1} \\
&\quad - \sum_{v=1}^{m} w_v\left[\frac{1}{6}(\Phi_{r-1}^{m-v+1} - \Phi_{r-1}^{m-v}) + \frac{4}{6}(\Phi_r^{m-v+1} - \Phi_r^{m-v}) + \frac{1}{6}(\Phi_{r+1}^{m-v+1} - \Phi_{r+1}^{m-v})\right].
\end{aligned} \tag{5.5}$$

The description of the BCs is

$$\frac{1}{6}\Phi_{r-1}^{m+1} + \frac{4}{6}\Phi_r^{m+1} + \frac{1}{6}\Phi_{r+1}^{m+1} = 0, \ r = 0, N,$$

where

$$\Phi_r^m = \Psi_r^m - V_r^m, r = -1 : 0 : N+1$$

and

$$\rho_r^m = h^2[U_r^m - \tilde{U}_r^m], r = 0,1,\dots,N.$$

Now using the inequality (5.1), we obtain

$$|\rho_r^m| = h^2|U_r^m - \tilde{U}_r^m| \le \varpi h^4.$$

Define $\rho^m = \max\{|\rho_r^m|; 0 \le r \le N\}$, $\varepsilon_r^m = |\Phi_r^m|$, and $\varepsilon^m = \max\{|\varepsilon_r^m|; 0 \le r \le N\}$.

When $m = 0$, Eq. (5.5) becomes

$$\left(\frac{a_1}{6} - \frac{\varsigma}{h^2}\right)\Phi_{r-1}^1 + \left(\frac{4a_1}{6} + \frac{2\varsigma}{h^2}\right)\Phi_r^1 + \left(\frac{a_1}{6} - \frac{\varsigma}{h^2}\right)\Phi_{r+1}^1 = \frac{\psi_1}{6}\Phi_{r-1}^0 + \frac{4\psi_1}{6}\Phi_r^0 + \frac{\psi_1}{6}\Phi_{r+1}^0 + \frac{\xi}{h^2}\rho_r^1,$$

where $r = 0,1,\dots,N$ and, through the IC, $\varepsilon^0 = 0$. Applying norms of Φ_r^1, ρ_r^1 and appropriately small h, we have

$$\varepsilon_r^1 \le \frac{3\xi}{a_1h^2 + 12\varsigma}\varpi h^4, \ r = 0,1,\dots,N.$$

We obtain ε_{-1}^1 and ε_{N+1}^1 through the BCs

$$\varepsilon_{-1}^1 \le \frac{15\xi}{a_1h^2 + 12\varsigma}\varpi h^4,$$

$$\varepsilon_{N+1}^1 \le \frac{15\xi}{a_1h^2 + 12\varsigma}\varpi h^4,$$

which implies

$$\varepsilon^1 \le \varpi_1 h^2, \tag{5.6}$$

where ϖ_1 is independent of h.

Now we use mathematical induction on m for the proof of this theorem. Suppose that $\varepsilon_r^i \le \varpi_i h^2$ is true for $i = 1(2)m$ and $\varpi = \max\{\varpi_i : i = 0 : 1 : m\}$, then from Eq. (5.5), we obtain the following:

$$\begin{aligned}
&\left(\frac{a_1}{6} - \frac{\varsigma}{h^2}\right)\Phi_{r-1}^{m+1} + \left(\frac{4a_1}{6} + \frac{2\varsigma}{h^2}\right)\Phi_r^{m+1} + \left(\frac{a_1}{6} - \frac{\varsigma}{h^2}\right)\Phi_{r+1}^{m+1} \\
&= \left[(w_0 - w_1)\left(\frac{1}{6}\Phi_{r-1}^m + \frac{4}{6}\Phi_r^m + \frac{1}{6}\Phi_{r+1}^m\right) + (w_1 - w_2)\left(\frac{1}{6}\Phi_{r-1}^{m-1} + \frac{4}{6}\Phi_r^{m-1} + \frac{1}{6}\Phi_{r+1}^{m-1}\right)\right. \\
&\quad \left. + (w_{m-1} - w_m)\left(\frac{1}{6}\Phi_{r-1}^1 + \frac{4}{6}\Phi_r^1 + \frac{1}{6}\Phi_{r+1}^1\right) + w_m\left(\frac{1}{6}\Phi_{r-1}^0 + \frac{4}{6}\Phi_r^0 + \frac{1}{6}\Phi_{r+1}^0\right)\right] + \frac{\xi}{h^2}\rho_r^{m+1}.
\end{aligned}$$

Again, using norms on Φ_r^m and ρ_r^m, we obtained

$$\varepsilon_r^{m+1} \le \frac{3\varpi h^4}{a_1h^2 + 12\varsigma}\left(\xi + \sum_{v=0}^{m-1}(w_v - w_{v+1})\right).$$

Similarly, we obtain the values of ε_{-1}^{m+1} and ε_{N+1}^{m+1} from the BCs

$$\varepsilon_{-1}^{m+1} \le \frac{15\varpi h^4}{a_1h^2 + 12\varsigma}\left(\xi + \sum_{v=0}^{m-1}(w_v - w_{v+1})\right)$$

$$\varepsilon_{N+1}^{m+1} \le \frac{15\varpi h^4}{a_1h^2 + 12\varsigma}\left(\xi + \sum_{v=0}^{m-1}(w_v - w_{v+1})\right).$$

Hence, for all m, we acquire

$$\varepsilon^{m+1} \le \varpi h^2. \tag{5.7}$$

In particular,

$$\tilde{p}(z,t) - P(z,t) = \sum_{r=-1}^{N+1} (V_r(t) - \Psi_r(t))\hat{B}_r(z).$$

Therefore, from Lemma 5.1 and inequality (5.7), we obtain

$$\|\tilde{p}(z,t) - P(z,t)\|_\infty \le \frac{5}{3}\varpi h^2. \tag{5.8}$$

Using Eq. (5.8), the inequality (5.4) gives

$$\|P(z,t) - p(z,t)\|_\infty \le \varpi_0 h^4 + \frac{5}{3}\varpi h^2 = \widetilde{\varpi} h^2,$$

where $\widetilde{\varpi} = \varpi_0 h^2 + \frac{5}{3}\varpi$. □

Theorem 4. *The TFFNE is convergent with BCs and IC.*

Proof. Let $p(z,t)$ be analytic solution and $P(z,t)$ be the approximate solutions for the TFFNE. Therefore, the above theorem and relation (3.3) justify that there exist constants $\widetilde{\varpi}$ and δ such that

$$\|p(z,t) - P(z,t)\|_\infty \le \delta(\Delta t)^2 + \widetilde{\varpi} h^2.$$

Hence, the proposed approach is second-order convergent in time and spatial directions. □

6 Analysis and presentation of numerical applications

Approximate results are revealed to show the perfection of the proposed methodology through $L_2(N)$, and $L_\infty(N)$ in this section that are defined as follows:

$$L_2(N) = \|P(z_r,t) - p(z_r,t)\|_2 = \sqrt{h\sum_{z=0}^{N} |p(z_r,t) - P(z_r,t)|^2},$$

$$L_\infty(N) = \|P(z_r,t) - p(z_r,t)\|_\infty = \max_{0\le r\le N} |p(z_r,t) - P(z_r,t)|,$$

and order of convergence μ is calculated using following formula as in [42]:

$$\mu = \frac{\log\left(\frac{L_\infty(N)}{L_\infty(N+1)}\right)}{\log\left(\frac{R(N+1)}{R(N)}\right)}.$$

Every application is examined by considering $AB(\gamma) = 1$.

Application 6.1. Consider the TFFNE for $q = 1$

$$\frac{\partial^\gamma p}{\partial t^\gamma} = \nu\frac{\partial^2 p}{\partial z^2} + \beta p(1-p)(p-\eta) + U(z,t), a \le z \le b,$$
$$0 \le t \le T,$$

with IC and BCs

$$\begin{cases} p(z,0) = 0, \\ p(0,t) = 0, \\ p(1,t) = 0, \end{cases} \tag{6.1}$$

and calculation of U is

$$U(z,t) = \frac{24}{1-\gamma}(z-z^2)t^4 E_{\gamma,5}\left[\frac{-\gamma t^\gamma}{1-\gamma}\right] + 2\nu t^4 - \beta[t^4(z-z^2)][1-t^4(z-z^2)][t^4(z-z^2)-\eta].$$

The analytic solution is $p(z,t) = (z-z^2)t^4$, where $\nu = \beta = 1$ and $\eta = 0.5$. Numerical results and absolute errors for different values of γ with $N = 100$, 60, and 80, $\Delta t = 0.001$, and $t = 1$ for Application 6.1 are presented in Tables 1 and 2. For various time levels and different choices of γ, the error norms are shown in Table 3. The order of convergence μ and the error norms along spatial and time directions are represent in Tables 4 and 5. The obtained results of proposed method and analytic solution have closed commitment as in Figure 1 for different values of time t with $\Delta t = 0.001$. Figure 2 for $N = 100$, $\Delta t = 0.001$, $\gamma = 0.255$, $t = 1$, and $z \in [0,1]$ shows the 3D plot of numerical and analytic solutions. The 2D and 3D error plots are presented in Figure 3 at $t = 1$.

Application 6.2. Consider the TFFNE for $q = 1$

Table 1: Errors norm at $t = 1$ of Application 6.1 for different values of γ with $\Delta t = 0.001$ and $N = 100$

	Numerical result			Absolute error	
z	Analytic solution	$\gamma = \frac{1}{4}$	$\gamma = \frac{3}{4}$	$\gamma = \frac{1}{4}$	$\gamma = \frac{3}{4}$
0.1	0.09000	0.08999	0.08999	1.67581×10^{-8}	1.82337×10^{-9}
0.2	0.16000	0.15999	0.15999	3.59818×10^{-8}	4.22148×10^{-9}
0.3	0.21000	0.20999	0.20999	5.00533×10^{-8}	6.53577×10^{-9}
0.4	0.24000	0.23999	0.23999	5.91083×10^{-8}	8.11400×10^{-9}
0.5	0.25000	0.24999	0.24999	6.22188×10^{-8}	8.66179×10^{-9}
0.6	0.24000	0.23999	0.23999	5.91083×10^{-8}	8.11401×10^{-9}
0.7	0.21000	0.20999	0.20999	5.00533×10^{-8}	6.53578×10^{-9}
0.8	0.16000	0.15999	0.15999	3.59818×10^{-8}	4.22150×10^{-9}
0.9	0.09000	0.08999	0.08999	1.85955×10^{-8}	1.82339×10^{-9}

Table 2: Errors norm at $t = 1$ for Application 6.1 with $\Delta t = 0.001$

z	Numerical result			Absolute error	
	Analytic result	$\gamma = \frac{2}{5}, N = 60$	$\gamma = \frac{4}{5}, N = 80$	$\gamma = \frac{2}{5}, N = 60$	$\gamma = \frac{4}{5}, N = 80$
0.1	0.09	0.08999	0.09000	1.64381×10^{-8}	4.63942×10^{-9}
0.2	0.16	0.15999	0.16000	3.18930×10^{-8}	8.01115×10^{-9}
0.3	0.21	0.20999	0.21000	4.44481×10^{-8}	1.02170×10^{-8}
0.4	0.24	0.23999	0.24000	5.25382×10^{-8}	1.15103×10^{-8}
0.5	0.25	0.24999	0.25000	5.53179×10^{-8}	1.19462×10^{-8}
0.6	0.24	0.23999	0.24000	5.25382×10^{-8}	1.15103×10^{-8}
0.7	0.21	0.20999	0.21000	4.44481×10^{-8}	1.02170×10^{-8}
0.8	0.16	0.15999	0.16000	3.18930×10^{-8}	8.01115×10^{-9}
0.9	0.09	0.08999	0.09000	1.64381×10^{-8}	4.63943×10^{-9}

$$\frac{\partial^\gamma p}{\partial t^\gamma} = \nu \frac{\partial^2 p}{\partial z^2} + \beta p(1-p)(p-\eta) + U(z,t), a \le z \le b, \quad 0 \le t \le T,$$

with IC and BCs

$$\begin{cases} p(z,0) = 0 \\ p(0,t) = t^{5\gamma}, \\ p(1,t) = \exp(-1)t^{5\gamma}, \end{cases} \tag{6.2}$$

and calculation of U is

$$\begin{aligned} U(z,t) = {} & \frac{\Gamma(5\gamma+1)}{1-\gamma}\exp(-z^2)t^{5\gamma}E_{\gamma,5\gamma+1}\left[\frac{-\gamma t^\gamma}{1-\gamma}\right] \\ & + 2\nu[t^{5\gamma}\exp(-z^2)][1-2z^2] \\ & - \beta[t^{5\gamma}\exp(-z^2)][1-t^{5\gamma}\exp(-z^2)] \\ & \times [t^{5\gamma}\exp(-z^2) - \eta]. \end{aligned}$$

$p(z,t) = t^{5\gamma}\exp(-z^2)$ is the analytic solution, where $\nu = \beta = 1$ and $\eta = 0.5$. The absolute errors and the numerical outcomes for various values of z of Application 6.2 setting $N = 200, 150, 180$, and different values of γ and Δt at $t = 1$ are presented in Tables 6 and 7. The error norms for $t = 0.1$, $t = 0.45$, and $t = 0.9$ are presented in Table 8 for different values of γ with $N = 175$, $\Delta t = 0.0005$, and $z \in [0,1]$. The error norms and order of convergence μ are calculated in Tables 9 and 10 in time and space directions, respectively. Figure 4 highlights the performance of analytic solution and numerical outcomes at different temporal directions. 3D plots in Figure 5 of exact and computational solution are presented. The 2D error graph and 3D error graph are shown in Figure 6. For different values of γ, the 2D graphs are shown in Figure 7 for exact and numerical solution.

Table 4: Order of convergence of Application 6.1 by taking various values of $\Delta t = \frac{1}{m}$ for fixed $h = \frac{1}{240}$ and $t = \frac{9}{10}$

γ	m	Proposed method		
		$L_\infty(N)$	$L_2(N)$	μ
0.32	5	0.00079894	0.00055564	⋯
	10	0.00026095	0.00018178	1.61432
	20	0.00007315	0.00005101	1.83478
	40	0.00001921	0.00001340	1.92919
	80	4.90113×10^{-6}	3.42021×10^{-6}	1.97054
0.72	20	9.29997×10^{-6}	5.78571×10^{-6}	⋯
	40	2.97431×10^{-6}	1.89860×10^{-6}	1.64467
	80	8.19033×10^{-7}	5.27495×10^{-7}	1.86056
	160	2.13139×10^{-7}	1.37757×10^{-7}	1.94213
	320	5.41608×10^{-8}	3.50547×10^{-8}	1.97647

Table 3: $L_\infty(N)$ and $L_2(N)$ for different values of γ with $\Delta t = \frac{1}{2{,}000}$, $N = 100$, and $0 \le z \le 1$ of Application 6.1

t	$L_\infty(N)$		$L_2(N)$	
	$\gamma = \frac{1}{4}$	$\gamma = \frac{3}{4}$	$\gamma = \frac{1}{4}$	$\gamma = \frac{3}{4}$
0.1	8.44658×10^{-14}	3.74539×10^{-13}	5.99959×10^{-14}	2.66203×10^{-13}
0.5	3.76645×10^{-11}	4.98079×10^{-10}	2.51322×10^{-11}	3.55499×10^{-10}
0.9	8.33893×10^{-9}	2.08303×10^{-10}	5.82464×10^{-9}	1.30658×10^{-10}

Table 5: Order of convergence with fixed $\Delta t = \frac{1}{1{,}000}$ for Application 6.1 and various choices of $h = \frac{1}{n}$ when $t = \frac{9}{10}$

		Proposed method		
γ	$m = n$	$L_\infty(N)$	$L_2(N)$	μ
0.32	5	0.000735108	0.000542213	⋯
	10	0.000258923	0.000180519	1.50543
	20	0.000073009	0.0000509183	1.82638
	40	0.000019199	0.0000133951	1.92705
	80	4.90060×10^{-6}	3.41986×10^{-6}	1.97000
0.72	20	9.27310×10^{-6}	5.77695×10^{-6}	⋯
	20	2.97235×10^{-6}	1.89788×10^{-6}	1.64145
	40	8.18914×10^{-7}	5.27449×10^{-7}	1.85982
	80	2.13134×10^{-7}	1.37755×10^{-7}	1.94195
	160	3.50549×10^{-8}	5.41613×10^{-8}	1.97643

Application 6.3. Consider the TFFNE for $q = 1$

$$\frac{\partial^\gamma p}{\partial t^\gamma} = \nu \frac{\partial^2 p}{\partial z^2} + \beta p(1-p)(p-\eta) + U(z,t), a \le z \le b, \quad 0 \le t \le T,$$

with IC and BCs

$$\begin{cases} p(z,0) = 0 \\ p(0,t) = 0, \\ p(1,t) = \dfrac{t^{2\gamma+2}}{2}, \end{cases} \tag{6.3}$$

and calculation of U is

$$\begin{aligned} U(z,t) = {} & \frac{\Gamma(2\gamma+3)}{1-\gamma} \sin\left[\frac{5z\pi}{6}\right] t^{2\gamma+2} E_{\gamma,2\gamma+3}\left[\frac{-\gamma t^\gamma}{1-\gamma}\right] \\ & + \nu\left[\frac{5\pi}{6}\right]^2 t^{2\gamma+2} \sin\left[\frac{5z\pi}{6}\right] \\ & - \beta\left[t^{2\gamma+2}\sin\left(\frac{5z\pi}{6}\right)\right]\left[1 - t^{2\gamma+2}\sin\left(\frac{5z\pi}{6}\right)\right] \\ & \times \left[t^{2\gamma+2}\sin\left(\frac{5z\pi}{6}\right) - \eta\right]. \end{aligned}$$

$p(z,t) = t^{2\gamma+2}\sin[\frac{5z\pi}{6}]$ is analytic solution, where $\nu = \beta = 1$ and $\eta = 0.5$. The computational results and absolute errors at different values of z establishing $\Delta t = 0.0002$,

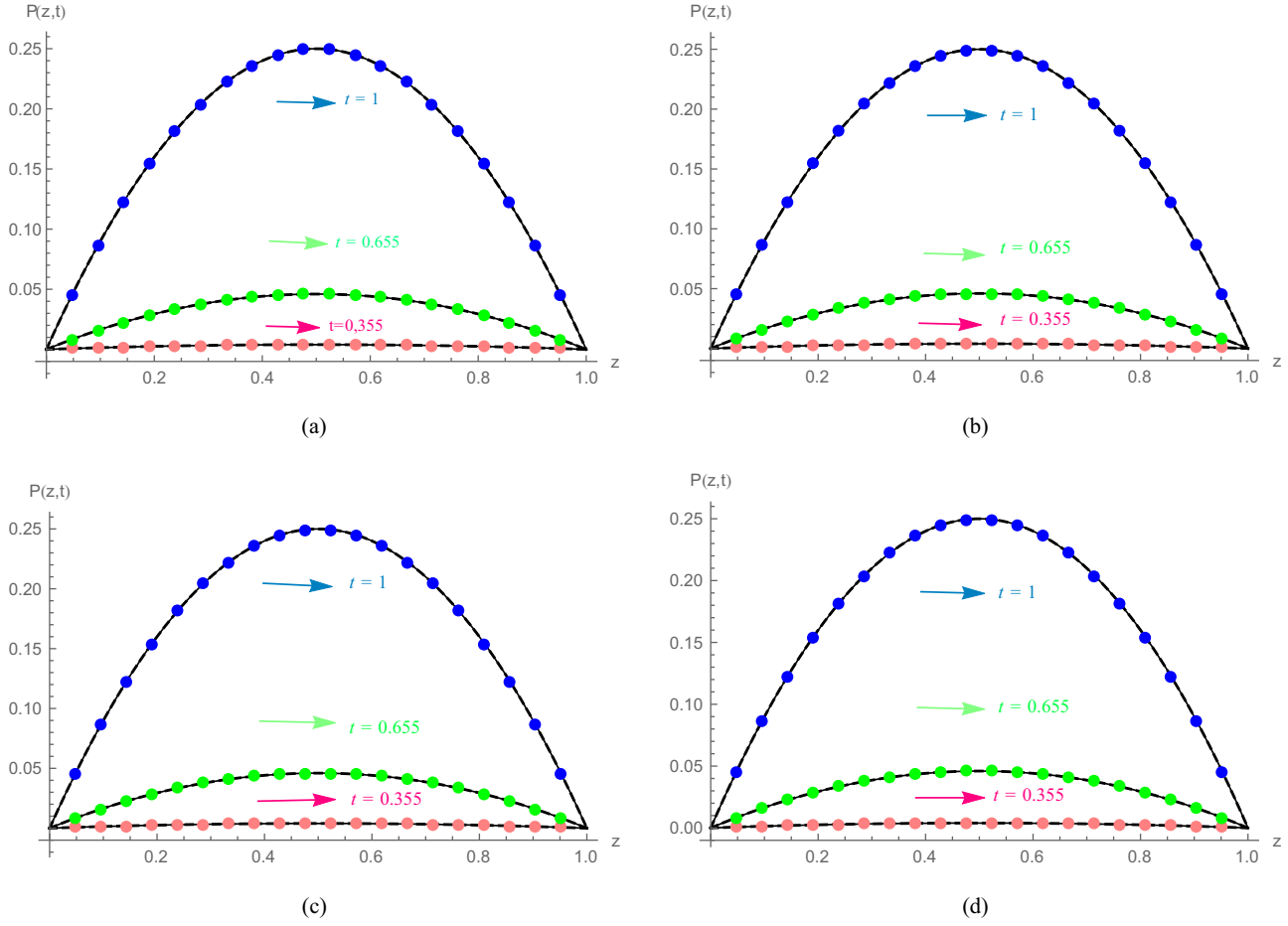

Figure 1: Approximate and analytic solutions with $\Delta t = 0.001$ of Application 6.1 at various time levels. (a) $N = 65$, $\gamma = 0.255$, (b) $N = 85$, $\gamma = 0.255$, (c) $N = 65$, $\gamma = 0.755$, and (d) $N = 85$, $\gamma = 0.755$.

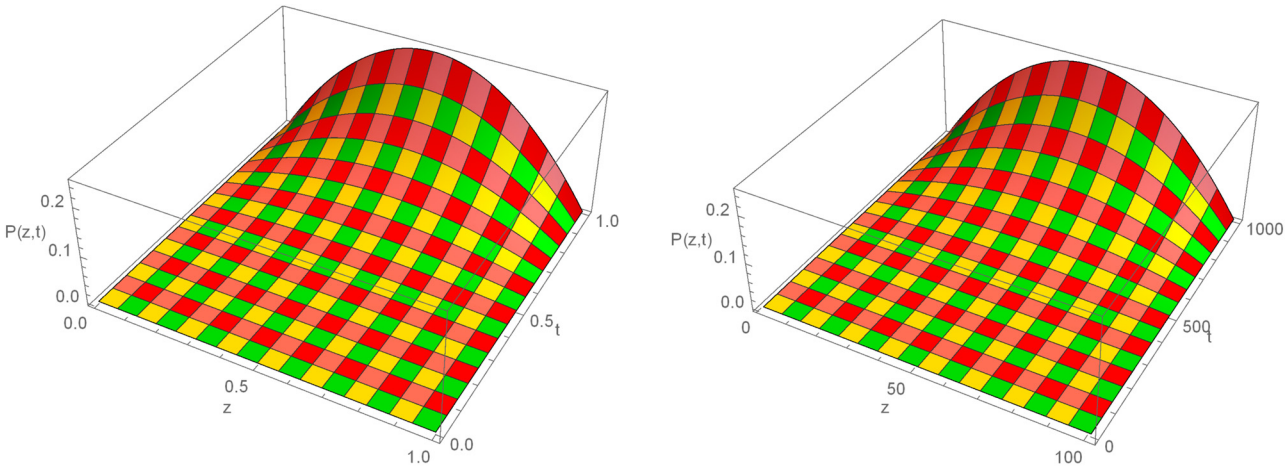

Figure 2: 3D Analytic solution and numerical solution images with $N = 100, t = 1, \gamma = 0.225, \Delta t = 0.001$ for Application 6.1 when $0 \le z \le 1$. (a) Analytic solution and (b) numerical solution.

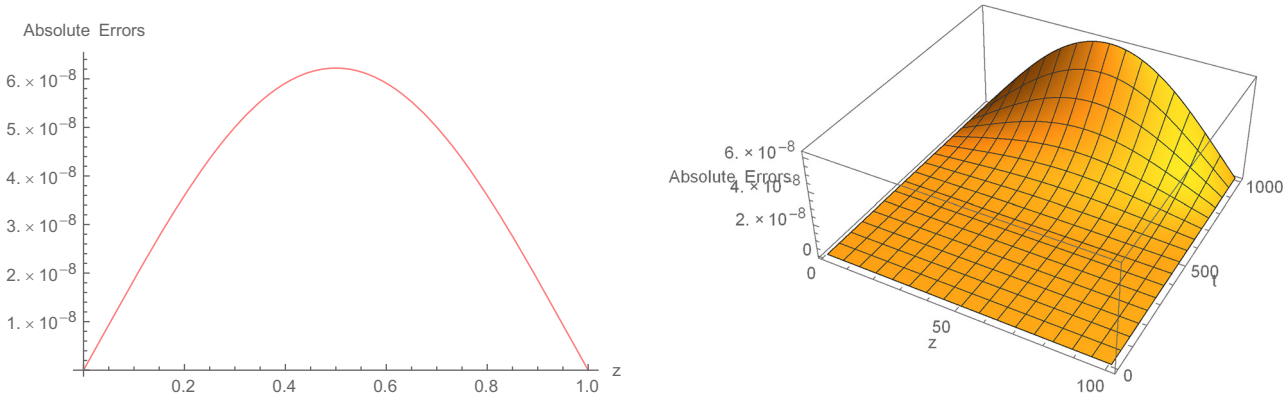

Figure 3: 2D and 3D Error images with $N = 100, t = 1, \gamma = 0.255, \Delta t = 0.001$ for Application 6.1 when $0 \le z \le 1$.

Table 6: Absolute errors of Application 6.2 for different values of γ when $\Delta t = \frac{1}{2{,}500}$ and $N = 200$ at $t = 1$

	$\gamma = \frac{1}{4}$			$\gamma = \frac{3}{4}$		
z	**Analytic solution**	**Numerical result**	**Error**	**Analytic solution**	**Numerical result**	**Error**
0.1	0.99005	0.99005	4.15062×10^{-7}	0.99005	0.99005	3.27136×10^{-7}
0.2	0.96079	0.96079	6.03925×10^{-7}	0.96079	0.96079	4.60952×10^{-7}
0.3	0.91393	0.91393	6.03551×10^{-7}	0.91393	0.91393	4.3518×10^{-7}
0.4	0.85214	0.85214	4.65706×10^{-7}	0.85214	0.85214	2.96126×10^{-7}
0.5	0.77880	0.77880	2.51426×10^{-7}	0.77880	0.77880	9.8195×10^{-8}
0.6	0.69768	0.69768	2.43833×10^{-8}	0.69768	0.69768	1.01663×10^{-7}
0.7	0.61263	0.61263	1.55997×10^{-7}	0.61263	0.61263	2.49878×10^{-7}
0.8	0.52729	0.52729	2.40588×10^{-7}	0.52729	0.52729	3.01590×10^{-7}
0.9	0.44486	0.44486	1.94746×10^{-7}	0.44486	0.44486	2.24421×10^{-7}

Table 7: Errors with $\Delta t = 0.0005$ of Application 6.2 at $t = 1$

	$\gamma = \frac{9}{20}, N = 150$			$\gamma = \frac{13}{20}, N = 180$		
z	**Analytic solution**	**Numerical result**	**Absolute error**	**Analytic solution**	**Numerical result**	**Absolute error**
0.1	0.99005	0.99005	6.69283×10^{-7}	0.99005	0.99005	4.16680×10^{-7}
0.2	0.96079	0.96079	1.01761×10^{-6}	0.96079	0.96079	5.90103×10^{-7}
0.3	0.91393	0.91393	1.00680×10^{-6}	0.91393	0.91393	5.61936×10^{-7}
0.4	0.85214	0.85214	7.61051×10^{-7}	0.85214	0.85214	3.90011×10^{-7}
0.5	0.77880	0.77880	3.86353×10^{-7}	0.77880	0.77880	1.42579×10^{-7}
0.6	0.69768	0.69768	6.68630×10^{-9}	0.69768	0.69768	1.08793×10^{-7}
0.7	0.61263	0.61263	3.14688×10^{-7}	0.61263	0.61263	2.96796×10^{-7}
0.8	0.52729	0.52729	4.51997×10^{-7}	0.52729	0.52729	3.65201×10^{-7}
0.9	0.44486	0.44486	3.57983×10^{-7}	0.44486	0.44486	2.73714×10^{-7}

Table 8: $L_\infty(N)$ and $L_2(N)$ error norms of Application 6.2 for various values of γ with $\Delta t = 0.0005$, $N = 160$ and $0 \le z \le 1$

	$L_\infty(N)$		$L_2(N)$	
t	$\gamma = \frac{15}{20}$	$\gamma = \frac{13}{20}$	$\gamma = \frac{15}{20}$	$\gamma = \frac{13}{20}$
0.1	4.58028×10^{-11}	5.22857×10^{-10}	2.67718×10^{-11}	3.02405×10^{-10}
0.45	6.76907×10^{-8}	1.40524×10^{-7}	3.95313×10^{-8}	8.10530×10^{-8}
0.9	5.41753×10^{-7}	6.69999×10^{-7}	3.17722×10^{-7}	3.87817×10^{-7}

$\Delta t = 0.0004$, $N = 500, 250, 200$, $\gamma = 0.25, 0.75$, and $t = 1$ for Application 6.3 are displayed in Tables 11 and 12. The error norms at $t = 0.15$, $t = 0.45$, and $t = 0.75$ are shown in Table 13 for different values of γ relying on $N = 175$, $\Delta t = 0.0005$, and $z \in [0, 1]$. The order of convergence μ and error norms are displayed in Tables 14 and 15 in time direction and space direction. Figure 8 provides a description of exact values and computational outcomes at different time levels. 3D precision of the existing approach is demonstrated by graphs of numerical results and analytical solutions in Figure 9. Figure 10 demonstrates the 2D and 3D error description, proving the method's efficiency. Figure 11 shows the graphs of analytic and numerical solutions with different values of γ.

Table 9: Order of convergence with various values of $\Delta t = \frac{1}{m}$ and fixed $h = \frac{1}{425}$ of Application 6.2 when $t = 1$

		Proposed method		
γ	m	$L_\infty(N)$	$L_2(N)$	μ
0.32	10	0.00129431	0.000890232	⋯
	20	0.000385587	0.000266753	1.74705
	40	0.000104669	0.0000725964	1.88123
	80	0.0000271709	0.0000188835	1.94569
	160	6.84355×10^{-6}	4.77689×10^{-6}	1.98925
0.72	10	0.00422254	0.00289823	⋯
	20	0.00158785	0.00109955	1.41103
	40	0.000480743	0.000334018	1.72374
	80	0.000132024	0.0000918791	1.86447
	160	0.0000345204	0.0000240582	1.93527

Table 10: Order of convergence with fixed $\Delta t = \frac{1}{425}$ and different choices of $h = \frac{1}{n}$ for Application 6.2 when $t = 1$

		Proposed method		
γ	n	$L_\infty(N)$	$L_2(N)$	μ
0.32	10	0.000246743	0.000146946	⋯
	20	0.0000630247	0.0000364128	1.96902
	40	0.0000150676	8.73748×10^{-6}	2.06447
	80	3.08653×10^{-6}	1.86245×10^{-6}	2.28739
	160	8.13505×10^{-7}	4.79792×10^{-7}	1.92376
0.72	5	0.000949882	0.000562242	⋯
	10	0.000235108	0.00014029	2.01443
	20	0.0000571683	0.0000333155	2.04004
	40	0.0000108836	6.87791×10^{-6}	2.39306
	80	3.92854×10^{-6}	2.48103×10^{-6}	1.47009

Table 11: Absolute errors of Application 6.3 for different values of γ when $\Delta t = \frac{1}{5{,}000}$ and $N = 500$ at $t = 1$

	$\gamma = \frac{1}{4}$			$\gamma = \frac{3}{4}$		
z	**Analytic solution**	**Numerical result**	**Error**	**Analytic solution**	**Numerical result**	**Error**
0.1	0.25882	0.25882	4.18042×10^{-7}	0.258819	0.258819	3.81068×10^{-7}
0.2	0.50000	0.49999	7.99684×10^{-7}	0.50000	0.49999	7.28667×10^{-7}
0.3	0.70711	0.70711	1.11019×10^{-6}	0.70711	0.70711	1.01104×10^{-6}
0.4	0.86602	0.86602	1.32205×10^{-6}	0.86603	0.86602	1.20349×10^{-6}
0.5	0.96593	0.96592	1.41713×10^{-6}	0.96593	0.96593	1.29023×10^{-6}
0.6	1.0000	0.99999	1.38544×10^{-6}	1.00000	0.99999	1.26263×10^{-6}
0.7	0.96593	0.96592	1.22299×10^{-6}	0.96593	0.96593	1.11692×10^{-6}
0.8	0.86603	0.86602	9.31030×10^{-7}	0.86603	0.86603	8.53002×10^{-7}
0.9	0.70711	0.70711	5.17630×10^{-7}	0.70711	0.70711	4.76236×10^{-7}

Table 12: Errors with $\Delta t = 0.0004$ of Application 6.3 at $t = 1$

	$\gamma = \frac{1}{4}, N = 250$			$\gamma = \frac{3}{4}, N = 200$		
z	**Analytic solution**	**Numerical result**	**Absolute error**	**Analytic solution**	**Numerical result**	**Absolute error**
0.1	0.25882	0.25882	1.67219×10^{-6}	0.25882	0.25882	2.40548×10^{-6}
0.2	0.50000	0.49999	3.19879×10^{-6}	0.50000	0.49999	4.60242×10^{-6}
0.3	0.70711	0.70710	4.44086×10^{-6}	0.70711	0.70710	6.39185×10^{-6}
0.4	0.86603	0.86602	5.28832×10^{-6}	0.86603	0.86602	7.61635×10^{-6}
0.5	0.96593	0.96592	5.66862×10^{-6}	0.96593	0.96592	8.17223×10^{-6}
0.6	1.00000	0.99999	5.54189×10^{-6}	1.00000	0.99999	8.00148×10^{-6}
0.7	0.96593	0.96592	4.89208×10^{-6}	0.96592	0.96592	7.07799×10^{-6}
0.8	0.86603	0.86602	3.72419×10^{-6}	0.86603	0.86602	5.40301×10^{-6}
0.9	0.70711	0.70711	2.07056×10^{-6}	0.70711	0.70710	3.01425×10^{-6}

Table 13: For Application 6.3 the error norms for different choices of γ when $\Delta t = \frac{1}{2{,}000}$, $N = 175$, and $0 \le z \le 1$

	$L_\infty(N)$		$L_2(N)$	
t	$\gamma = \frac{7}{20}$	$\gamma = \frac{17}{20}$	$\gamma = \frac{7}{20}$	$\gamma = \frac{17}{20}$
0.15	6.75807×10^{-8}	7.61423×10^{-9}	4.82336×10^{-8}	5.44521×10^{-9}
0.45	1.3548×10^{-6}	4.92105×10^{-7}	9.66342×10^{-7}	3.5158×10^{-7}
0.75	5.61998×10^{-6}	3.57981×10^{-6}	4.00719×10^{-6}	2.55469×10^{-6}

Table 14: Order of convergence with fixed $h = \frac{1}{425}$ and taking different values of $\Delta t = \frac{1}{m}$ for Application 6.3 when $t = 1$

		Proposed method		
γ	m	$L_\infty(N)$	$L_2(N)$	μ
0.32	10	0.00398681	0.00268049	⋯
	20	0.00134032	0.000906445	1.57266
	40	0.00038427	0.000260435	1.80238
	80	0.00010198	0.0000691498	1.91383
	160	0.0000254313	0.0000172158	2.00361
0.72	10	0.00588917	0.00396847	⋯
	20	0.00210514	0.00142527	1.48415
	40	0.000623368	0.000422822	1.75576
	80	0.000168799	0.000114559	1.88478
	160	0.0000431439	0.0000292582	1.96808

7 Conclusion

In the current article, through a numerical strategy based on CBSFs, an effective solution to the TFFNE involving the

Table 15: Order of convergence with different values of $h = \frac{1}{n}$ and $\Delta t = \frac{1}{625}$ for Application 6.3 when $t = 1$

		Proposed method		
γ	n	$L_\infty(N)$	$L_2(N)$	μ
0.32	10	0.00358166	0.00256983	⋯
	20	0.000896036	0.00064259	1.99900
	40	0.000223318	0.000159799	2.00446
	80	0.0000544964	0.0000390408	2.03487
	160	0.0000122878	8.84781×10^{-6}	2.14893
0.72	10	0.00336907	0.00241909	⋯
	20	0.000842198	0.000604066	2.00012
	40	0.000208842	0.000149542	2.01175
	80	0.0000499815	0.0000358637	2.06295
	160	0.0000102688	7.44260×10^{-6}	2.28312

ABTFD has been achieved. The ABTFD has been approximated using the usual finite difference formulation, and CBSFs are used for interpolating the solution curve in the spatial direction. The approach suggested in the current study is novel and offers an acceptable level of accuracy. The proposed scheme is stable unconditionally having second-order temporal and spatial convergence. The current algorithm is shown to be more effective, simple, and allowable when implemented to numerical application. Future work should focus on expanding the scope, analyzing the algorithm's properties in more detail, and exploring its applicability in real-world scenarios.

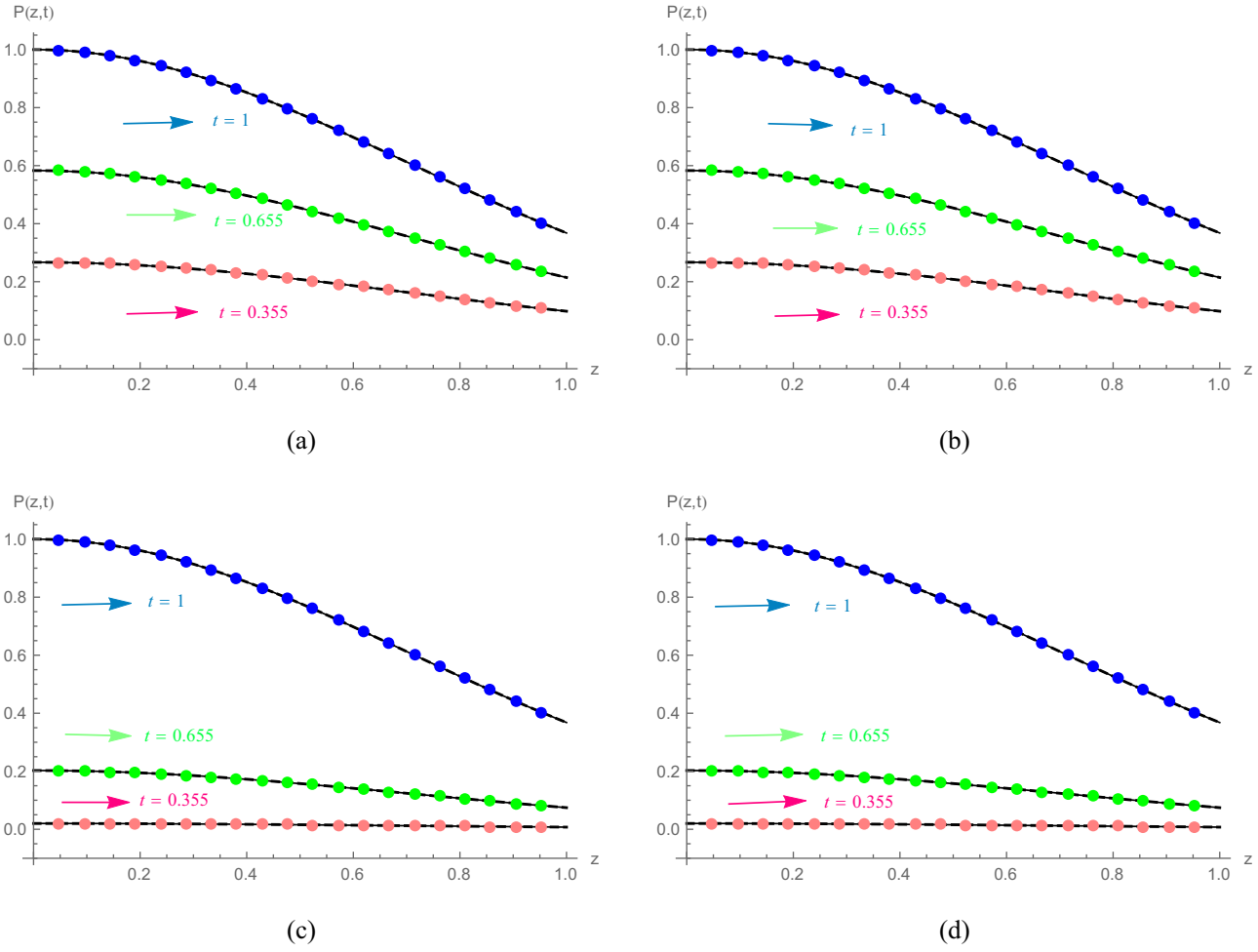

Figure 4: At different time levels, the approximate and analytic solutions for Application 6.2. (a) $N = 65$, $\gamma = 0.255$, and $\Delta t = 0.001$, (b) $N = 85$, $\gamma = 0.255$, and $\Delta t = 0.001$, (c) $N = 65$, $\gamma = 0.755$, and $\Delta t = 0.001$, and (d) $N = 85$, $\gamma = 0.755$, and $\Delta t = 0.001$.

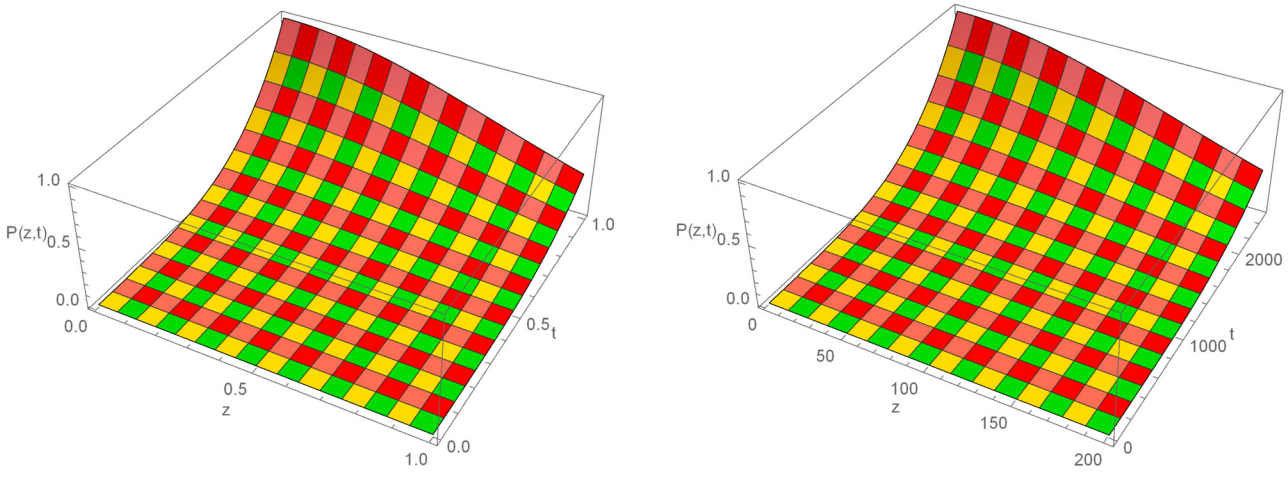

Figure 5: For Application 6.2, the 3D analytic and numerical solutions images when $N = 200$, $t = 1$, $\gamma = 0.75$, $\Delta t = \frac{1}{2{,}500}$, and $0 \le z \le 1$. (a) Analytic solution and (b) numerical solution.

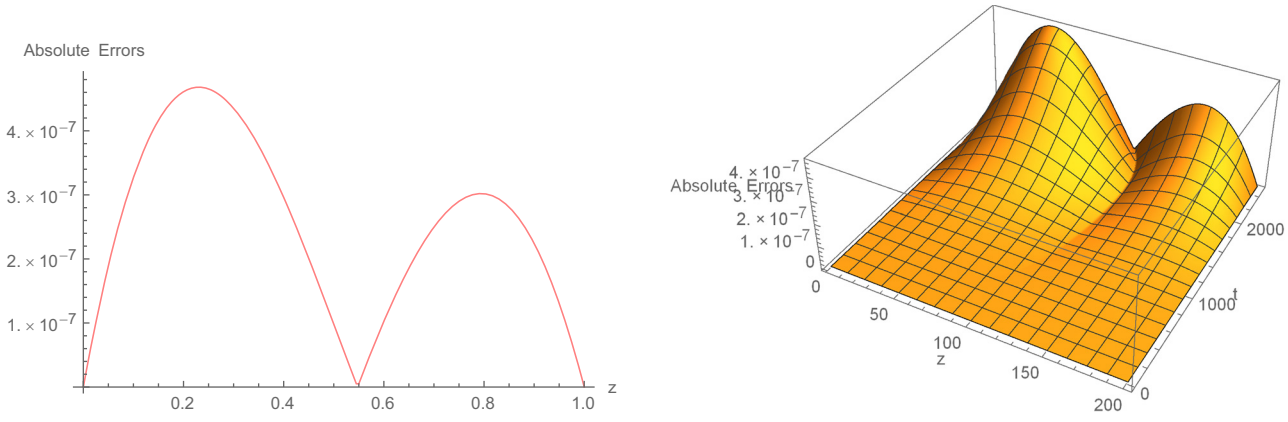

Figure 6: 2D and 3D error graphs with $N = 200$, $t = 1$, $\gamma = 0.75$, and $\Delta t = \frac{1}{2{,}500}$ for Application 6.2 when $0 \le z \le 1$.

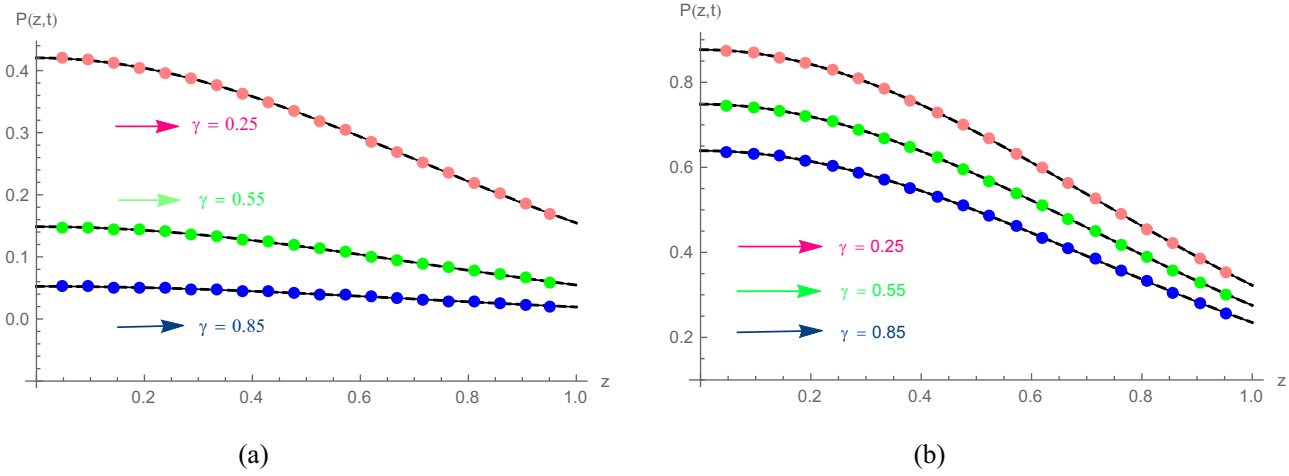

Figure 7: 2D Graph with different values of γ and $N = 100$, and $\Delta t = \frac{1}{1000}$ for Application 6.2 when $0 \le z \le 1$. (a) $t = 0.5$ and (b) $t = 0.9$.

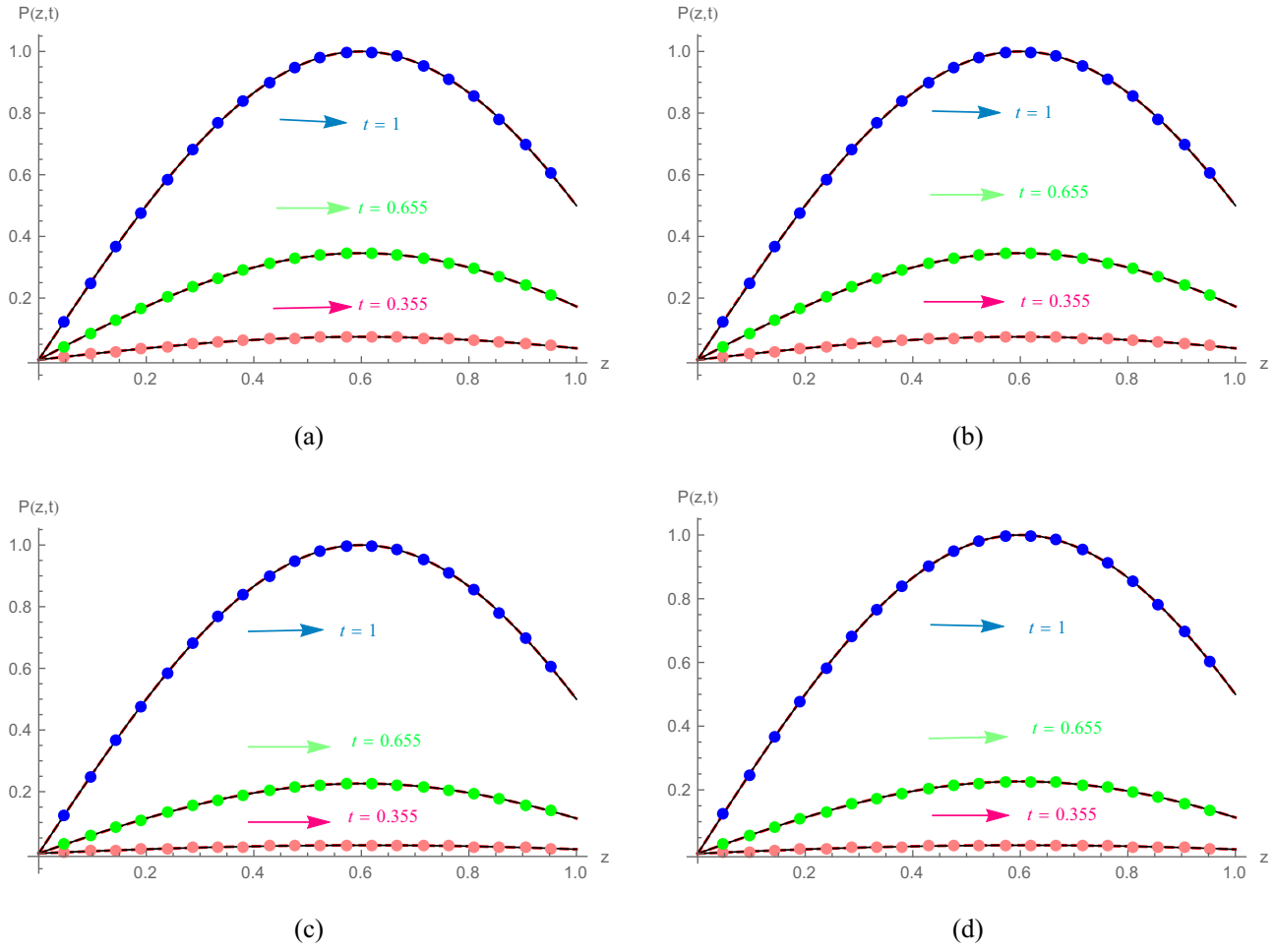

Figure 8: For Application 6.3, the analytic and numerical solutions at various temporal direction. (a) $N = 65$, $\gamma = 0.255$, and $\Delta t = 0.001$, (b) $N = 85$, $\gamma = 0.255$, and $\Delta t = 0.001$, (c) $N = 65$, $\gamma = 0.755$, and $\Delta t = 0.001$, and (d) $N = 85$, $\gamma = 0.755$, and $\Delta t = 0.001$.

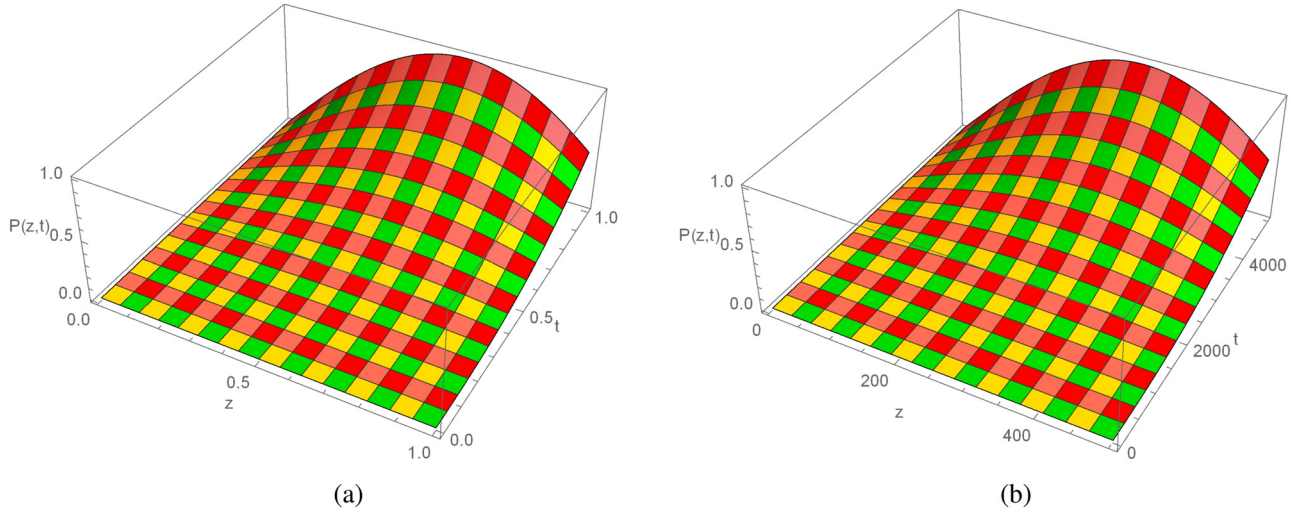

Figure 9: 3D Analytic solution and numerical solution images with $N = 500$, $t = 1$, $\gamma = 0.25$, and $\Delta t = 0.0002$ for Application 6.3 when $0 \le z \le 1$. (a) Analytic solution and (b) numerical solution.

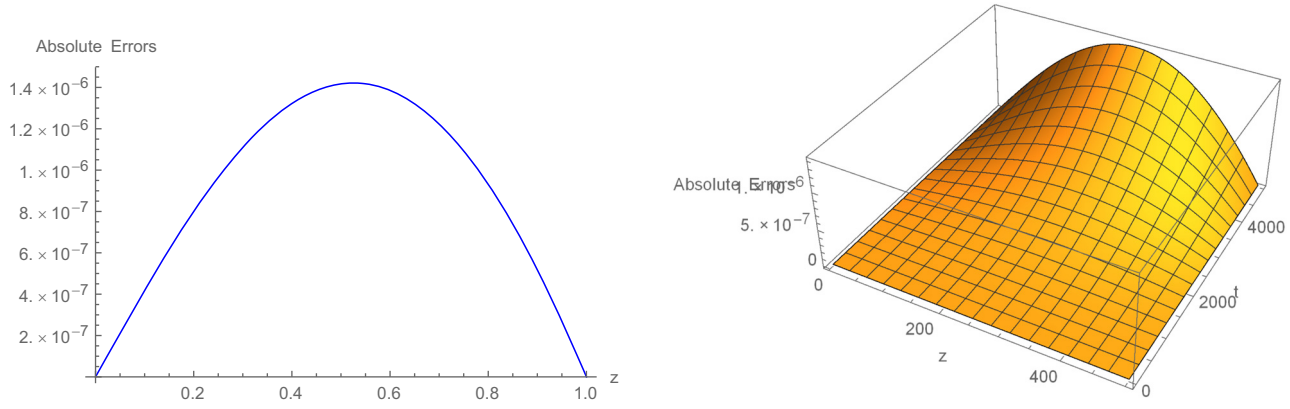

Figure 10: For Application 6.3, the 2D and 3D error plots when $N = 500$, $t = 1$, $\gamma = 0.25$, $\Delta t = 0.0002$, and $0 \le z \le 1$.

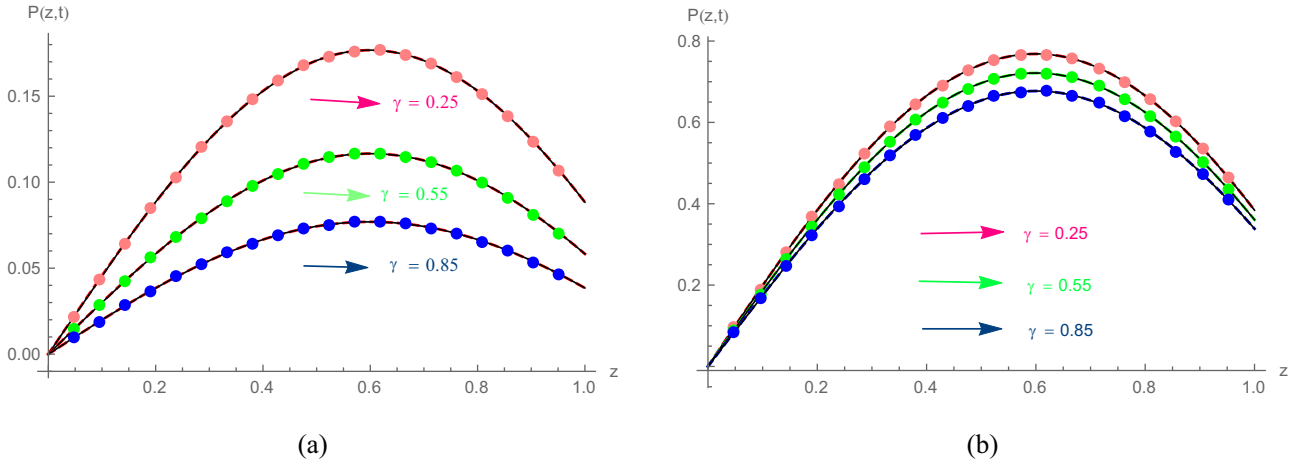

Figure 11: 2D Graph with different values of γ and $N = 100$, and $\Delta t = \frac{1}{1{,}000}$ for Application 6.3 when $0 \le z \le 1$. (a) $t = 0.5$ and (b) 0.9.

Acknowledgments: The authors extend their appreciation to the Deanship of Scientific Research at Northern Border University, Arar, KSA for funding this research work through the project number NBU-FFR-2024-885-01.

Funding information: The authors extend their appreciation to the Deanship of Scientific Research at Northern Border University, Arar, KSA for funding this research work through the project number NBU-FFR-2024-885-01.

Author contributions: All authors have accepted responsibility for the entire content of this manuscript and approved its submission.

Conflict of interest: The authors state no conflict of interest.

References

[1] Abbas M, Aslam S, Abdullah SA, Riaz MB, Gepreel KA. An efficient spline technique for solving time-fractional integro-differential equations. Heliyon. 2023;9(9):e19307.

[2] Caputo M, Fabrizio M. A new definition of fractional derivative without singular kernel. Progress Fract Differ Appl. 2015;1(2):73–85.

[3] Atangana A, Baleanu D. New fractional derivatives with nonlocal and non-singular kernel: theory and application to heat transfer model. Therm Sci. 2016;20(2):763–9.

[4] Nonnenmacher TF, Metzler R. Applications of fractional calculus ideas to biology. In Applications of fractional calculus in physics. Singapore: World Scientific; 1998.

[5] Scalas E, Gorenflo R, Mainardi F. Fractional calculus and continuous-time finance. Phys A Stat Mech Appl. 2000;284(1-4):376–84.

[6] Laskin N. Fractional market dynamics. Phys A Stat Mech Appl. 2000;287(3–4):482–92.

[7] Ibrahim RW, Darus M. Differential operator generalized by fractional derivatives. Miskolc Math Notes. 2011;12(2):167–84.
[8] Tarasov VE. Interpretation of fractional derivatives as reconstruction from sequence of integer derivatives. Fundamenta Informaticae. 2017;151(1–4):431–42.
[9] Tarasova VV, Tarasov VE. Marginal utility for economic processes with memory. Almanah Sovremennoj Nauki i Obrazovaniya [Almanac of Modern Science and Education]. 2016;7:108–13.
[10] Li Y, Chen Y, Podlubny I. Mittag-Leffler stability of fractional order nonlinear dynamic systems. Automatica. 2009;45(8):1965–9.
[11] Blair GS. The role of psychophysics in rheology. J Colloid Sci. 1947;2(1):21–32.
[12] Ding C, Cao J, YChen Y. Fractional-order model and experimental verification for broadband hysteresis in piezoelectric actuators. Nonlinear Dyn. 2019;98:3143–53.
[13] Metzler R, Glckle WG, Nonnenmacher TF. Fractional model equation for anomalous diffusion. Phys A Stat Mech Appl. 1994;211(1):13–24.
[14] FitzHugh R. Impulses and physiological states in theoretical models of nerve membrane. Biophys J. 1961;1(6):445–66.
[15] Nagumo J, Arimoto S, Yoshizawa S. An active pulse transmission line simulating nerve axon. Proc IRE. 1962;50(10):2061–70.
[16] Injrou S, Karroum R, Deeb N. Various exact solutions for the conformable time-fractional generalized FitzHugh–Nagumo equation with time-dependent coefficients. Int J Differ Equ. 2021;2021:8888989.
[17] Ramani P, Khan AM, Suthar DL, Kumar D. Approximate analytical solution for non-linear FitzHugh–Nagumo equation of time fractional order through fractional reduced differential transform method. Int J Appl Comput Math. 2022;8(2):61.
[18] Gordon P. Nonsymmetric difference equations. J Soc Ind Appl Math. 1965;13(3):667–73.
[19] Dehghan M, Heris JM, Saadatmandi A. Application of semi-analytic methods for the FitzHugh–Nagumo equation, which models the transmission of nerve impulses. Math Methods Appl Sci. 2010;33(11):1384–98.
[20] Keskin Y and Oturan G. Reduced differential transform method for partial differential equations. Int J Nonlinear Sci Numer Simul. 2009;10(6):741–9.
[21] Momani S, Odibat Z. Analytical solution of a time-fractional Navier–Stokes equation by Adomian decomposition methods. Appl Math Comput. 2006;177(2):488–94.
[22] Ragab AA, Hemida KM, Mohamed MS, Abdel SMA. Solution of time-fractional Navier–Stokes equation by using homotopy analysis method. Gen Math Notes. 2012;13(2):13–21.
[23] Ghanbari B, Günerhan H, Srivastava HM. An application of the Atangana–Baleanu fractional derivative in mathematical biology a three-species predator-prey model. Chaos Solitons Fractals. 2020;138:109–910.
[24] Amin N, Abbas M, Baleanu D, Iqbal MK, Riaz MB. Redefined extended cubic B-spline functions for numerical solution of time-fractional telegraph equation. Comput Model Eng Sci. 2021;127(1):361–84.
[25] Liu F, Turner I, Anh V, Yang Q, Burrage K. A numerical method for the fractional FitzHugh-Nagumo monodomain model. ANZIAM J. 2012;54:608–29.
[26] Shih M, Momoniat E, Mahomed FM. Approximate conditional symmetries and approximate solutions of the perturbed FitzHugh–Nagumo equation. J Math Phys. 2005;46:023503.
[27] Abbasbandy S. Soliton solutions for the FitzHugh–Nagumo equation with the homotopy analysis method. Appl Math Model. 2008;32:2706–14.
[28] Kakiuchi N, Tchizawa K. On an explicit duck solution and delay in the FitzHugh–Nagumo equation. J Differ Equ. 1997;141:327–39.
[29] Schonbek ME. Boundary value problems for the FitzHugh–Nagumo equations. J Differ Equ. 1978;30:119–47.
[30] Yanagida E. Stability of travelling front solutions of the FitzHugh–Nagumo equations. Math Comput Model. 1989;12:289–301.
[31] Namjoo M, Zibaei S. Numerical solutions of FitzHugh-Nagumo equation by exact finite-difference and NSFD schemes. Comput Appl Math. 2018;37:1395–411.
[32] Angadi LM. Numerical solution of Fitz Hugh-Nagumo equations by wavelet-based lifting schemes. J Stat Math Eng. 2023;9(1):55–64.
[33] Olmos D, Shizgal BD. Pseudospectral method of solution of the FitzHugh Nagumo equation. Math Comput Simul. 2009;79:2258–78.
[34] Abdulazeez ST, Modanli M. Analytic solution of fractional order Pseudo-Hyperbolic Telegraph equation using modified double Laplace transform method. Int J Math Comput Eng. 2023;1(1):105–14.
[35] Singh R, Mishra J, Gupta VK. The dynamical analysis of a tumor growth model under the effect of fractal fractional Caputo–Fabrizio derivative. Int J Math Comput Eng. 2023;1(1):115–26.
[36] Baleanu D, Arshad S, Jajarmi A, Shokat W, Ghassabzade FA, Wali M. Dynamical behaviours and stability analysis of a generalized fractional model with a real case study. J Adv Res. 2023;48:157–73.
[37] Ali H, Kamrujjaman M, Islam MS. Numerical computation of FitzHugh-Nagumo equation: A novel Galerkin finite element approach. Int J Math Res. 2020;9(1):20–7.
[38] Jiwari R, Gupta RK, Kumar V. Polynomial differential quadrature method for numerical solutions of the generalized FitzHugh–Nagumo equation with time-dependent coefficients. Ain Shams Eng J. 2014;5(4):1343–50.
[39] Mittag-Leffler GM. Sur la nouvelle fonction $E_a(x)$. C R Acad Sci Paris. 1903;137:554–58.
[40] Poulin JR. Calculating infinite series using Parseval's identity. Orono. ME 04469: The University of Maine; 2020.
[41] Khalid N, Abbas M, Iqbal MK, Baleanu D. A numerical investigation of Caputo time fractional Allen-Cahn equation using redefined cubic B-spline functions. Adv Differ Equ. 2020;1:158.
[42] Shafiq M, Abbas M, Abdullah FA, Majeed A, Abdeljawad T, Alqudah MA. Numerical solutions of time fractional Burgers equation involving Atangana–Baleanu derivative via cubic B-spline functions. Results Phys. 2022;34:105–244.
[43] Akram T, Abbas M, Abualnaja KM, Iqbal A, Majeed A. An efficient numerical technique based on the extended cubic B-spline functions for solving time fractional Black-Scholes model. Eng Comput. 2022;38(2):1705–16.
[44] Majeed A, Kamran M, Asghar N, Baleanu D. Numerical approximation of inhomogeneous time fractional Burgers?Huxley equation with B-spline functions and Caputo derivative. Eng Comput. 2022;38(2):885–900.

[45] Boyce WE, DiPrima RC, Meade DB. Elementary differential equations and boundary value problems. Hoboken, New Jersey, USA: John Wiley & Sons. 2021.
[46] Iqbal MK, Abbas M, Nazir T, Ali N. Application of new quintic polynomial B-spline approximation for numerical investigation of Kuramoto-Sivashinsky equation. Adv Differ Equ. 2020;1:1–21.
[47] Akram T, Abbas M, Ali A. A numerical study on time fractional Fisher equation using an extended cubic B-spline approximation. J Math Comput Sci. 2021;22(1):85–96.
[48] Akram T, Abbas M, Ismail AI, Ali NHM, Baleanu D. Extended cubic B-splines in the numerical solution of time fractional telegraph equation. Adv Differ Equ. 2019;1:1–20.
[49] Kadalbajoo MK, Arora P. B-spline collocation method for the singular-perturbation problem using artificial viscosity. Comput Math Appl. 2009;57(4):650–63.
[50] Hall CA. On error bounds for spline interpolation. J Aapprox Theory. 1968;1(2):209–18.
[51] de Boor C. On the convergence of odd-degree spline interpolation. J Approx Theory. 1968;1(4):452–63.